Anion Permeation in Ca^{2+}-activated Cl^- Channels

Zhiqiang Qu and H. Criss Hartzell

From the Department of Cell Biology, Emory University School of Medicine, Atlanta, Georgia 30322

ABSTRACT Ca^{2+}-activated Cl channels ($Cl_{Ca}Cs$) are an important class of anion channels that are opened by increases in cytosolic [Ca^{2+}]. Here, we examine the mechanisms of anion permeation through $Cl_{Ca}Cs$ from *Xenopus* oocytes in excised inside-out and outside-out patches. $Cl_{Ca}Cs$ exhibited moderate selectivity for Cl over Na: $P_{Na}/P_{Cl} = 0.1$. The apparent affinity of $Cl_{Ca}Cs$ for Cl was low: $K_d = 73$ mM. The channel had an estimated pore diameter >0.6 nm. The relative permeabilities measured under bi-ionic conditions by changes in E_{rev} were as follows: $C(CN)_3 > SCN > N(CN)_2 > ClO_4 > I > N_3 > Br > Cl >$ formate $> HCO_3 >$ acetate = F > gluconate. The conductance sequence was as follows: $N_3 > Br > Cl > N(CN)_2 > I > SCN > COOH > ClO_4 >$ acetate $> HCO_3 = C(CN)_3 >$ gluconate. Permeant anions block in a voltage-dependent manner with the following affinities: $C(CN)_3 > SCN = ClO_4 > N(CN)_2 > I > N_3 > Br > HCO_3 > Cl >$ gluconate > formate > acetate. Although these data suggest that anionic selectivity is determined by ionic hydration energy, other factors contribute, because the energy barrier for permeation is exponentially related to anion hydration energy. $Cl_{Ca}Cs$ exhibit weak anomalous mole fraction behavior, implying that the channel may be a multi-ion pore, but that ions interact weakly in the pore. The affinity of the channel for Ca^{2+} depended on the permeant anion at low [Ca^{2+}] (100–500 nM). Apparently, occupancy of the pore by a permeant anion increased the affinity of the channel for Ca^{2+}. The current was strongly dependent on pH. Increasing pH on the cytoplasmic side decreased the inward current, whereas increasing pH on the external side decreased the outward current. In both cases, the apparent pKa was voltage-dependent with apparent pKa at 0 mV = ~9.2. The channel may be blocked by OH^- ions, or protons may titrate a site in the pore necessary for ion permeation. These data demonstrate that the permeation properties of $Cl_{Ca}Cs$ are different from those of CFTR or ClC-1, and provide insights into the nature of the $Cl_{Ca}C$ pore.

KEY WORDS: voltage clamp • chloride current • selectivity • pH • anomalous mole fraction

INTRODUCTION

Ca^{2+}-activated Cl channels ($Cl_{Ca}Cs$)[1] serve a number of important well defined physiological functions in a variety of cell types. These functions include epithelial secretion (Begenisich and Melvin, 1998; Morris, 1999), olfactory transduction (Kurahashi and Yau, 1994), regulation of vascular tone (Hirakawa et al., 1999), neuronal excitability (Frings et al., 1999), and fast block to polyspermy in certain eggs (Jaffe and Cross, 1986). Despite the physiological importance of Ca^{2+}-activated Cl current ($I_{Cl.Ca}$), the channels underlying this current remain incompletely understood at both the molecular and biophysical levels. Although a family of putative $Cl_{Ca}Cs$ has been cloned (Cunningham et al., 1995; Gruber et al., 1998, 1999; Gandhi et al., 1998; Ji et al., 1998), the behavior of this cloned "CLCA" channel does not resemble $Cl_{Ca}Cs$ from many native cells including those we have studied in *Xenopus* oocytes (Hartzell et al., 1997; Machaca and Hartzell, 1998, 1999a,b; Kuruma and Hartzell, 1999, 2000). However, there may be several subtypes of Ca^{2+}-activated chloride channels, and the CLCA family may comprise one subtype. The observations that $Cl_{Ca}C$ single-channel conductances range from 1 to 50 pS and that $I_{Cl.Ca}$ in different cell types can be regulated differently suggests that there is more than one type of channel (see Kuruma and Hartzell, 2000).

We have been interested in $I_{Cl.Ca}$ in *Xenopus* oocytes because this cell type has long served as a model system for studying $Cl_{Ca}Cs$ and because the channels in *Xenopus* oocytes in many ways resemble those in cardiac muscle (Collier et al., 1996), smooth muscle (Hirakawa et al., 1999), secretory epithelial cells (Begenisich and Melvin, 1998), and neurons (Frings et al., 1999). As one of the prime examples of $Cl_{Ca}Cs$, it is important to understand thoroughly the gating, permeation, and regulation of the *Xenopus* oocyte channel. We and others have previously characterized its gating properties and regulation by Ca^{2+} and voltage (Kuruma and Hartzell, 1999, 2000; Machaca and Hartzell, 1999a; Callamaras and Parker, 2000), but the mechanisms of anion permeation through this channel have not yet been thoroughly investigated.

There appear to be several common features of anion-selective channels that have been studied. First, anion channels are relatively nonselective among anions.

Address correspondence to H. Criss Hartzell, Department of Cell Biology, Emory University School of Medicine, 1648 Pierce Drive, Atlanta, GA 30322-3030. Fax: (404) 727-6256; E-mail: criss@cellbio.emory.edu

[1]*Abbreviations used in this paper:* CFTR, cystic fibrosis transmembrane regulator; $Cl_{Ca}C$, Ca^{2+}-activated Cl^- channel; ClC, voltage-gated Cl^- channel family; $I_{Cl.Ca}$, Ca^{2+}-activated Cl^- current; GHK, Goldman-Hodgkin-Katz.

Whereas the prototypic voltage-gated cation channels like *Shaker* exhibit >100-fold selectivity between Na^+ and K^+ that differ in radius by <0.4 Å, most anion channels exhibit ~10-fold selectivity between Cl and SCN that differ in radius by ~0.7 Å (Hille, 1992). Second, permeant anions are frequently open channel blockers (Fahlke et al., 1997a; Rychkov et al., 1998; Dawson et al., 1999). Third, anion channels sometimes exhibit anomalous mole fraction behavior, where the conductance or E_{rev} exhibits a minimum or maximum in the presence of mixtures of Cl and a substitute anion (Linsdell et al., 1997b; Rychkov et al., 1998). Anomalous mole fraction behavior is usually interpreted as evidence for a multi-ion pore (Hille, 1992; but see Nonner et al., 1998).

Various anion channels exhibit important differences superimposed on these common themes. Recently, anion permeation has been studied most thoroughly in three cloned anion channels: CFTR, the Cl channel responsible for cystic fibrosis (Tabcharani et al., 1997; Linsdell et al., 1997a,b; Linsdell and Hanrahan, 1998; Mansoura et al., 1998; Smith et al., 1999; Dawson et al., 1999); members of the ClC family, particularly ClC-0 and ClC-1 (Rychkov et al., 1996; Fahlke et al., 1997a,b; Rychkov et al., 1998); and the $GABA_A$ receptor (Bormann et al., 1987; Wang et al., 1999). CFTR and the ClCs differ significantly in their permeation properties. The CFTR pore recently has been described as a polarizable tunnel that stabilizes a partially dehydrated ion as it traverses the channel (Smith et al., 1999). The anion selectivity sequence for CFTR is a lyotropic series that reflects the dehydration energy of the permeant anion: the more easily dehydrated anions (the ones with the largest radii) are more permeant. In contrast, the permeability selectivity for ClC-1 is not lyotropic. This suggests that the ClC-1 channel may be more specialized than CFTR. In addition to having different anion selectivity sequence, ClC-1 exhibits a number of special features. For example, external Cl acts as a ligand regulating Cl permeation in ClC-1 (Pusch et al., 1995; Rychkov et al., 1996).

Although the relative permeabilities of $Cl_{Ca}Cs$ have been published for a limited number of anions by several labs (see DISCUSSION), a detailed examination of the permeation mechanisms of $Cl_{Ca}Cs$ has not been published. In this study, we have examined the permeation properties of $Cl_{Ca}Cs$ from *Xenopus* oocytes in excised patches. We find that the properties of these channels differ in a number of important aspects from both CFTR and ClC-1.

MATERIALS AND METHODS

Isolation of Xenopus Oocytes

Stage V–VI oocytes were harvested from adult *Xenopus laevis* females (*Xenopus* I) as described by Dascal (1987). *Xenopus* were anesthetized by immersion in tricaine (1.5 g/liter). Ovarian follicles were removed, cut into small pieces, and digested in normal Ringer's with no added calcium containing ~2 mg/ml collagenase type IA for 2 h at room temperature. The oocytes were extensively rinsed with normal Ringer's, placed in L-15 medium (GIBCO BRL), and stored at 18°C. Oocytes were used 1–4 d after isolation. On the day of recording, oocytes were placed in a hypertonic solution (200 mM potassium aspartate, 20 mM KCl, 1 mM $MgCl_2$, 10 mM EGTA, 10 mM HEPES, pH 7.2 with KOH) for 10–15 min to facilitate manual removal of the vitelline membrane, and then they were placed in normal Ringer's solution until use.

Electrophysiological Methods

Recordings were performed using both the inside-out and outside-out excised configurations of the patch-clamp technique. Patch pipets were made of borosilicate glass (Sutter Instrument Co.), pulled by a Sutter P-2000 puller, and fire-polished. Patch pipets had resistances of 6–8 MΩ. Unless noted, they were filled with the standard solution (see *Solutions*). The bath was grounded via a 3-M KCl-agar bridge connected to a Ag-AgCl reference electrode. Solution changes were performed by gravity-feed of the 300-μl chamber at a speed of ~10 ml/min or by positioning the patch at the end of a battery of sewer pipes having 100-μm internal diameter. Patches were usually obtained from the animal hemisphere because $Cl_{Ca}Cs$ are concentrated here (Gomez-Hernandez et al., 1997; Machaca and Hartzell, 1998). The amplitude of $I_{Cl,Ca}$ varied significantly between patches as well as between oocytes from different batches. Liquid junction potentials were measured for each experimental solution as described previously (Neher, 1992) and corrected after the recordings. Instantaneous currents were measured 1 ms after the onset of the voltage pulse. In experiments in which the patch pipet solution contained a substitute anion, a 3-M KCl salt bridge was placed between the Ag-AgCl wire and the pipet.

Data were usually acquired by an Axopatch 200A amplifier controlled by Clampex 7.0.1 via a Digidata 1200 analogue-to-digital and digital-to-analogue converter (Axon Instruments). For some experiments, the data were acquired by Curcap 3.0 (W. Goolsby, Emory University) and voltages were delivered by a Challenger DB stimulator (W. Goolsby, Emory University). Experiments were conducted at room temperature (20–24°C).

Solutions

The standard solution contained 150 mM NaCl, 10 mM HEPES or TES, pH 7.2, and 0.1 mM $CaCl_2$. We did not observe any differences between TES and HEPES. When Cl was substituted with another anion, NaCl was replaced with NaX, where X is the substitute anion. One exception was the anion $C(CN)_3$ which was available only as the potassium salt. With inside-out patches, to be certain that the currents studied were Ca^{2+}-dependent, we measured the current in a zero-Ca^{2+} solution (150 mM NaCl, 10 mM HEPES, 10 mM EGTA, pH 7.2) at the start and end of the experiment. If the Ca^{2+}-independent current was >5% of the total current in Ca^{2+} (a rare situation), the patch was discarded or, if necessary, the Ca^{2+}-dependent current was obtained by subtracting the Ca^{2+}-independent current from the total current. For outside-out patches, it was not practical to change the Ca^{2+} bathing the cytosolic face. Therefore, with outside-out patches, the identity of the current as a Cl current was verified at the start and end of an experiment by bathing the external face of the patch in solution in which all Cl was replaced with SO_4. Patches were not analyzed if the outward current under these conditions was >5% of the current with symmetrical Cl.

We encountered problems with a few of the substitute anion solutions. NaSCN and $KC(CN)_3$ solutions appeared to deteriorate over time. With solutions aged >1 wk, the E_{rev} shift was often less than that obtained with fresh solutions. For this reason, we tried to use solutions <1 wk old. NaF solutions were problematic because F binds Ca^{2+} with nanomolar affinity. However, with fresh NaF, we were able to measure Ca^{2+}-dependent currents, but

in aged solutions, there was no Ca^{2+}-activated current. Because of our uncertainty about the $[Ca^{2+}]$ in NaF solutions, we are not confident interpreting the conductance data, however, the permeability data should not be affected by variations in $[Ca^{2+}]$, provided there is a measurable current. Experiments with HCO_3 were performed at pH 8, but because the atmospheric CO_2 was not controlled, the actual $[HCO_3]$ might have varied somewhat during an experiment.

In some experiments, we buffered the free $[Ca^{2+}]$ to submicromolar concentrations with EGTA using the method of Tsien and Pozzan (1989). Typically, zero-Ca^{2+} solution contained 150 mM NaCl, 10 mM EGTA, and 10 mM HEPES, pH 7.2. High Ca^{2+} solution contained 150 mM NaCl, 10 mM Ca^{2+}-EGTA, and 10 mM HEPES, pH 7.2. The stock solution of Ca^{2+}-EGTA in this solution was made by the pH-metric method described by Tsien and Pozzan (1989). Working solutions having different free Ca^{2+} were prepared by mixing the zero-Ca^{2+} solution with the high Ca^{2+} solution in various ratios. The free $[Ca^{2+}]$ was calculated from the equation $[Ca^{2+}] = K_d \times [Ca^{2+}\text{-EGTA}] / [\text{EGTA}]$, where K_d is the K_d of EGTA ($K_d = 1.0 \times 10^{-7}$ M at 24°C, pH 7.3, ionic strength 0.16 M). The calculated Ca^{2+} concentrations were confirmed in each solution by fura-2 (Molecular Probes) measurements using an LS-50B luminescence spectrophotometer (Perkin Elmer). Most data are expressed as molar concentrations, but for several experiments, the data was expressed as Cl activity, which was determined using a Cl-sensitive electrode (Fisher Scientific).

Display and Analysis of Data

For the calculations and graphical presentation, we used Origin 6.0 software (Microcal). Curve fitting was performed using the iterative algorithms in Origin. Results are presented as means ± SEM, and *n* refers to the number of patches in each experiment.

Relative halide permeability of the channels was determined by measuring the shift in E_{rev} upon changing the solution on one side of the membrane from one containing 150 mM Cl to another with 150 mM X, where X is the substitute anion. The permeability ratio was estimated using the Goldman-Hodgkin-Katz (GHK) equation (Hille, 1992).

$$P_x/P_{Cl} = \exp(\Delta E_{rev}F/RT), \quad (1)$$

where ΔE_{rev} is the difference between the reversal potential with the test anion X and that observed with symmetrical Cl ($E_{rev} = 0$ mV), and F, R, and T have their normal thermodynamic meanings. In our calculations of relative anion permeability, we assumed that cation permeability was negligible. Clearly, this could introduce an error into the relative permeability ratios if relative cation permeability is high. As presented in RESULTS, we find that P_{Na}/P_{Cl} is ~0.1. If cation permeability is independent of the permeability of the permeant anion, this error will be largest for anions with low permeability. We have not corrected for cation permeability because Franciolini and Nonner (1994a) have shown that cation permeability in another type of Cl channel is tightly coupled to the relative permeability of the permeant anion. If this was also true in the $Cl_{Ca}C$ channel, corrections based on the assumption that cation permeability is independent of anion permeability would also be in error and would significantly confuse the situation. Thus, until we know whether cation and anion permeabilities are coupled in the $Cl_{Ca}C$, we have adopted the simplification of not applying any correction.

RESULTS

Relative Na^+ Permeability of $Cl_{Ca}Cs$

In our previous experiments on $Cl_{Ca}Cs$, we used NMDG as the only monovalent cation to minimize cation currents. However, it was not possible to obtain NMDG salts of some of the anions we used in this paper. For this reason, we first determined the relative Na permeability of $Cl_{Ca}Cs$ in inside-out excised patches. The pipet solution contained 150 mM NaCl, 10 mM HEPES, pH 7.2, and 0.1 mM $CaCl_2$. The bath solution contained a different [NaCl]. Osmolarity was adjusted by the addition of sucrose. The data are expressed in terms of Cl activities measured using a Cl-sensitive electrode.

Fig. 1 A shows I–V curves from a typical inside-out patch exposed on the cytoplasmic side to different $[NaCl]_i$. Conductance in the inward direction increased significantly with increasing [NaCl], as would be expected if the current was carried predominantly by Cl ions. On average, E_{rev} shifted +44 mV with a 10-fold change in Cl activity (Fig. 1 B, solid symbols). This value is smaller than the +58-mV shift predicted if the channel was permeable exclusively to Cl. In Fig. 1 B, the heavy solid line shows the shift in E_{rev} predicted from the Goldman-Hodgkin-Katz (GHK) equation assuming that Cl is 10 times more permeant than Na ($P_{Na}/P_{Cl} = 0.1$).

Because these measurements were performed on macroscopic currents rather than single channels, the question may arise whether some of the current may be carried by other kinds of channels in the patch. Ca^{2+}-independent currents do not contribute because, with <10 nM Ca^{2+} present, the conductance of the patch was negligible (Fig. 1 A, trace labeled EGTA). Furthermore, it seems unlikely that Ca^{2+}-dependent cation or nonselective channels contribute because, in the absence of permeant anions, we see no evidence of Ca^{2+}-activated currents (not shown).

Anion channels often exhibit P_{Na}/P_{Cl} ratios as high as 0.2 (Hille, 1992; and see DISCUSSION). Franciolini and Nonner (1994a) have shown that background Cl channels in hippocampal neurons are permeable to large organic cations such as triethanolamine. To determine whether $Cl_{Ca}Cs$ are also permeable to large cations, we repeated the experiment of Fig. 1 A, except that Na in both cytoplasmic and external solutions was replaced with NMDG. On average, E_{rev} shifted +50 mV with a 10-fold change in Cl activity (Fig. 1 B, open symbols). The light solid line in Fig. 1 B shows the GHK prediction with $P_{NMDG}/P_{Cl} = 0.06$. This value suggested that the channel might be slightly permeable to NMDG. However, the difference between the NMDG data and the line predicted for a purely Cl-selective channel (dashed line) is rather small and may not be significant.

Affinity of $Cl_{Ca}Cs$ for Cl

The experiments in Fig. 1 can also be used to estimate the apparent affinity of the $Cl_{Ca}C$ for Cl. The average chord conductance between E_{rev} and $E_{rev} - 50$ mV was plotted versus the Cl activity in Fig. 1 C. The patch current and conductance increased with increasing Cl activity, and saturated near 300 mM. The data were fit well by an equation of the form $G = G_{max} \cdot a_{Cl} / K_d + a_{Cl}$, with an apparent K_d for Cl of 73 mM.

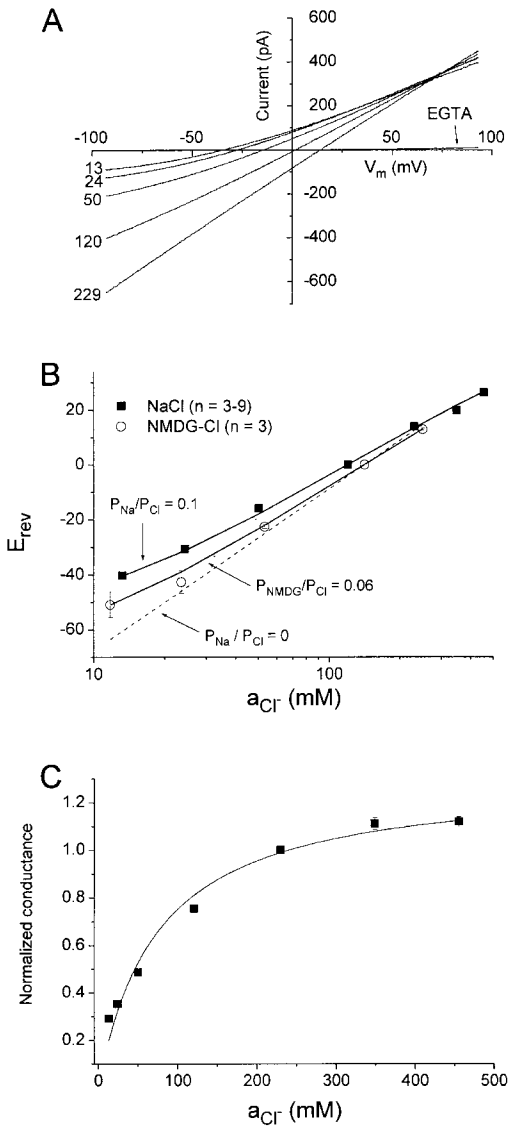

FIGURE 1. Sodium permeability and Cl affinity of $I_{Cl,Ca}$. An inside-out excised patch from a *Xenopus* oocyte was exposed to different cytoplasmic [NaCl] concentrations and the I–V relationship determined by 250-ms duration voltage ramp from −100 to +100 mV. (A) I–V curves. The external (pipet) solution contained 150 mM NaCl, 10 mM HEPES, 0.1 mM $CaCl_2$, pH 7.2. The cytoplasmic (bath) solution contained the same solution except that the NaCl concentration was varied. The osmolarity of each solution was adjusted to 665 mOsM by addition of sucrose, except for the 350- and 460-mM solutions, which had higher osmolarities and contained no sucrose. The Cl activities (a_{Cl}) measured by Cl-sensitive electrodes are indicated at the left end of each I–V curve. The I–V curve labeled EGTA was obtained in symmetrical 150-mM NaCl solutions, except that Ca^{2+} in the cytoplasmic solution was omitted and 10 mM Na_2EGTA, pH 7.2, was added. (B) Change in E_{rev} as a function of a_{Cl}. The reversal potentials from experiments shown in A were corrected for liquid junction potentials. (Solid squares) NaCl solutions. Each data point is the mean of three to nine patches. The heavy solid line is calculated from the Goldman-Hodgkin-Katz equation ($\Delta E_{rev} = 25.7 \cdot \ln[(Na_o + Cl_i \cdot P_{Cl}/P_{Na})/(Na_i + Cl_o \cdot P_{Cl}/P_{Na})]$) with P_{Na}/P_{Cl} = 0.1. (Open squares) NMDG-Cl solutions; n = 3. Thin line is calculated from the Goldman-Hodgkin-Katz equation with P_{NMDG}/P_{Cl} = 0.06. The dashed line is calculated assuming that the channel is selectively permeable only to Cl. (C) Affinity of the channel for Cl. The chord conductance was measured from I–V curves between E_{rev} and E_{rev} − 50 mV and plotted versus a_{Cl}. The line is a fit to the equation $G = G_{max} \cdot a_{Cl} / K_d + a_{Cl}$, with an apparent K_d for Cl of 73 mM.

Anionic Selectivity of $Cl_{Ca}Cs$

Inside-Out Patches. To determine the anionic selectivity of $Cl_{Ca}Cs$, we measured the I–V relationships of excised patches under asymmetric anionic conditions. The I–V relationship was determined by voltage ramps from −100 to +100 mV. The pipet always contained 150 mM NaCl, 10 mM TES, pH 7.2, and 0.1 mM $CaCl_2$. The bath contained the same solution, but Cl was replaced with various substitute anions. Measurements with a substitute anion were always bracketed by measurements in symmetrical Cl; patches were discarded from analysis if the two measurements in Cl did not agree in E_{rev} within ±1 mV and chord conductances within ±10%. Fig. 2 shows typical I–V curves for excised patches exposed to different cytoplasmic anions. The average results for all anions tested are shown in Fig. 3. Fig. 3 A shows the relative permeability (P_x/P_{Cl}) calculated from the shift in E_{rev} using the GHK equation (see MATERIALS AND METHODS), and Fig. 3 B shows the relative chord conductance (G_x/G_{Cl}) measured between E_{rev} and E_{rev} − 50 mV. The selectivity of the channel estimated from P_x/P_{Cl} follows the lyotropic sequence:

$$C(CN)_3 > SCN > N(CN)_2 > ClO_4 > I > N_3 > Br > Cl > COOH \text{ (formate)} > HCO_3 > AC \text{ (acetate)} = F > \text{gluconate}.$$

However, the relative conductances exhibited a different sequence:

$$N_3 > Br > Cl > N(CN)_2 > I > SCN > COOH > ClO_4 > AC > HCO_3 = C(CN)_3 > \text{gluconate} > F.$$

Whereas the permeabilities reflect the ability of the ion to enter the channel pore, the conductance reflects the ability of the anion to traverse the entire length of the channel. When there is a difference in the relative permeabilities and conductances, this suggests that ions that readily enter the channel may not pass through as easily. Discrepancies between relative permeabilities and relative conductances often reflect the binding of a permeant ion to a site in the pore. The ratio of relative permeabilities to relative conductances provides an estimate of the relative affinity of the anion for a binding site in the channel (Läuger, 1973; Halm and Frizzell, 1992). The sequence of affinities (Fig. 3 C) is

$$C(CN)_3 > SCN = ClO_4 > N(CN)_2 > F > I > N_3 > Br > HCO_3 > Cl > \text{gluconate} > COOH > AC.$$

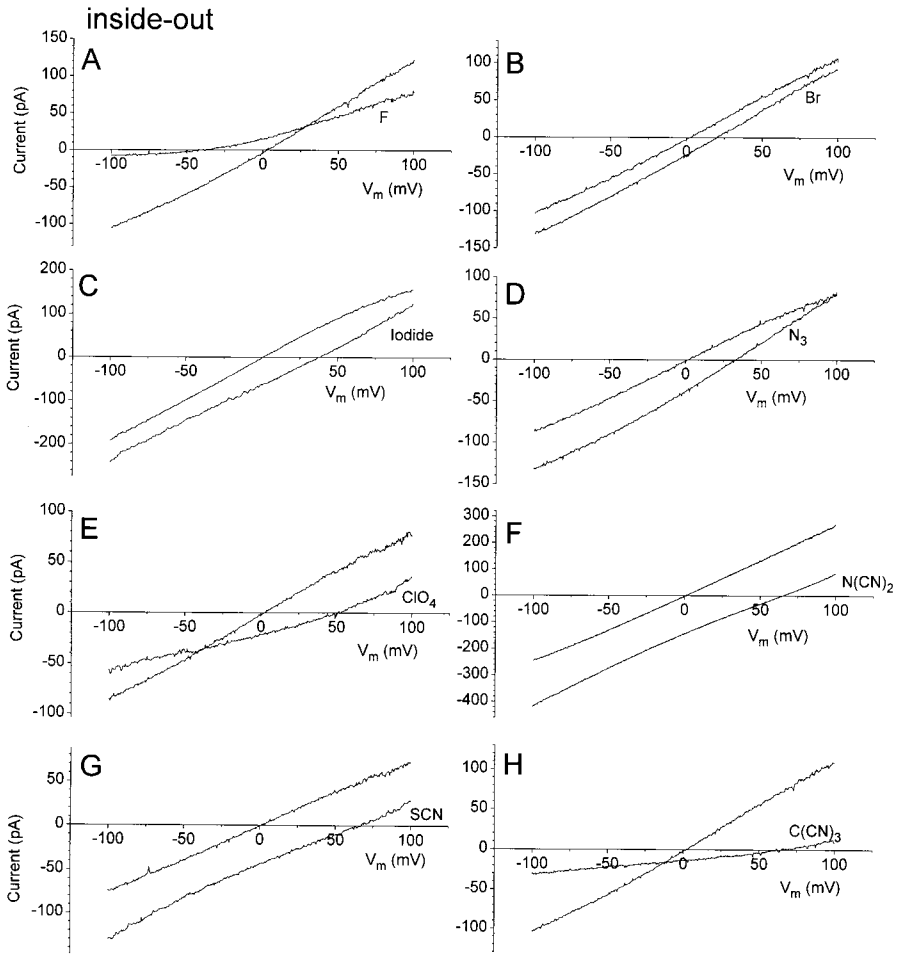

FIGURE 2. I–V relationships of $I_{Cl,Ca}$ in inside-out patches with different cytoplasmic anions. The external solution contained 150 mM NaCl, 10 mM TES, pH 7.2, and 0.1 mM $CaCl_2$. The cytoplasmic solution was shifted between this solution (unlabeled traces) and 150 mM NaX, 10 mM TES, pH 7.2, 0.1 mM $CaCl_2$, where X is the substitute anion (labeled traces). The traces have not been corrected for liquid junction potentials. (A) Fluoride; (B) bromide; (C) iodide; (D) azide; (E) perchlorate; (F) dicyanamide; (G) thiocyanate; and (H) tricyanomethanide (potassium salt). The I–V curves were obtained by voltage ramps from −100 to +100 mV.

Outside-Out Patches. Because it has been reported that the CFTR Cl channel exhibits asymmetry in the permeability to certain anions (Linsdell and Hanrahan, 1998), we compared the permeability ratios when we replaced external Cl with substitute anions in outside-out patches (Fig. 4). We obtained statistically indistinguishable P ratios and G ratios for the anions tested, regardless of whether the substituted anion was external or cytoplasmic (Fig. 5, A and B).

Symmetrical Substitutes. We also examined relative conductances and permeabilities in inside-out patches exposed to symmetrical substitute anions. In these experiments, the G_x/G_{Cl} and P_x/P_{Cl} ratios were determined by comparing symmetrical substitute anion solutions to Cl in the cytoplasmic solution and the substitute anion in the external solution. The permeability ratios for symmetrical substitution were statistically the same as those obtained with asymmetrical substitution (Fig. 5 A). In contrast, the conductance ratios were higher for symmetrical substitutes, especially for substitutes that had a high affinity for the channel (Fig. 5 B). These data suggest that the flux of anions through the channel is greater when the same anion is present on both sides of the membrane compared with the asymmetrical condition. This suggests that the channel has two anion binding sites and, that when these sites are occupied by different anions, conductance is less than when both sites are occupied with the same anion.

Mechanisms of Anion Permeation. Smith et al. (1999) have suggested that the CFTR Cl channel can be considered as a simple dielectric channel in the lipid bilayer. To determine whether the $Cl_{Ca}C$ behaves similarly, we performed an analysis identical to that described by Smith et al. (1999). We first calculated the permeabilities of the various anions relative to $C(CN)_3$ from the data in Fig. 3 A. From the following equation

$$P_x/P_{C(CN)3} = \exp[-\Delta(\Delta G)_{barrier}/RT], \qquad (2)$$

we calculated the relative energy barrier heights ($\Delta(\Delta G)_{barrier}$) for the various anions. Fig. 6 A plots $\Delta(\Delta G)_{barrier}$ versus the reciprocal of the ionic radius. With the exception of gluconate, acetate, bicarbonate, and formate, the data are well-fit by a straight line. Thus, for the well behaved anions, the larger the anion, the more permeant it is. Because the hydration energy of an ion with distributed charge is inversely related to its radius, these data suggest that $Cl_{Ca}Cs$, like CFTR, dis-

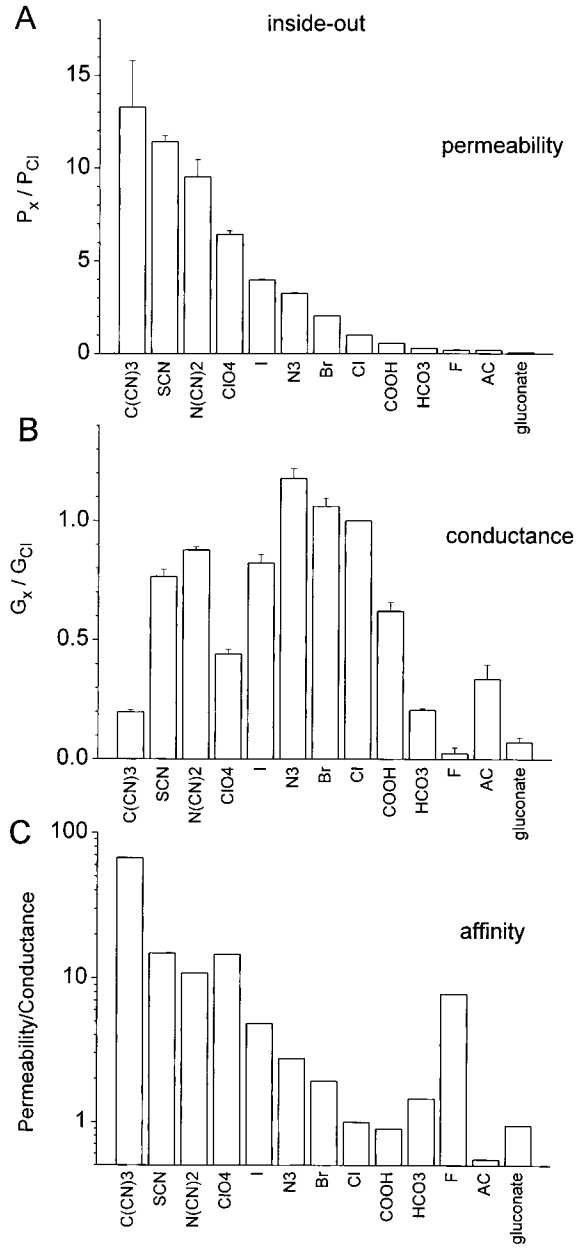

FIGURE 3. Anionic selectivity of $I_{Cl,Ca}$ in inside-out patches. (A) Relative permeabilities. The E_{rev}s corrected for liquid junction potential were obtained from experiments such as those shown in Fig. 2. These values were used to calculate relative permeabilities from the Goldman-Hodgkin-Katz equation (see MATERIALS AND METHODS). (B) Relative conductance was determined by measuring the conductance with the substitute anion between E_{rev} and E_{rev} − 50 mV, and dividing this value by the conductance with symmetrical Cl. (C) Relative affinities. Relative affinities of the channel for the ions were determined by dividing the relative permeability by the relative conductance. n = 3–5 patches per substitute anion.

criminate between anions based at least partly on their hydration energies. Based on data like these, Smith et al. (1999) calculate that the CFTR pore has an effective dielectric constant of ~19. A similar analysis for $Cl_{Ca}Cs$ (Fig. 6 B) estimates the dielectric constant of this pore to be 20.7. This value was estimated from the slope of the solvation energy line that was obtained by subtracting $\Delta(\Delta G)_{barrier}$ from the absolute value of the Born energy of hydration (ΔG_{hyd}), calculated from the following equation with ε = 80 (water),

$$\Delta G_{hyd} = -(K/2)\ (l/r)\ (1 - 1/\varepsilon), \qquad (3)$$

where r is the ion radius, ε is the dielectric constant, and K has a value of 138.6 kJ·nm/mol. The difference between the $\Delta(\Delta G)_{barrier}$ and ΔG_{hyd} represents the solvation energy provided by the channel. The slope of this line provides an estimate of the dielectric constant of the channel.

This analysis is not entirely satisfying for several reasons. First, one is forced to discard anions such as gluconate, acetate, bicarbonate, and formate that do not fit the line in Fig. 6 A. Although one can explain the anomalous behavior of these anions by the fact that their electronic charge is asymmetrically distributed so that their hydration energies are greater than predicted by their radius, information provided by these ions is ignored. Second, because $\Delta(\Delta G)_{barrier}$ is an exponential function of the $P_x/P_{C(CN)3}$ ratio and is small relative to ΔG_{hyd}, the conclusions provided by this analysis are insensitive to rather large differences in actual $P_x/P_{C(CN)3}$ ratios. This could tend to obscure possibly significant differences between different anion channels. Third, one would predict that, if the channel was a simple dielectric tunnel, the energy barrier height should be linearly related to the free energy of hydration of the ion. However, this is clearly not the case (Fig. 6 C). The barrier height is an exponential function of hydration energy.

Fig. 6 D shows another way of representing the data that provides some additional insight into mechanisms of anion permeation in these channels. Fig. 6 D plots the P_x/P_{Cl} ratio for inside-out patches as a function of the free energy of hydration. There are several interesting features about this relationship. The permeabilities describe a smooth curve, but Cl seems to be at a pivotal point, separating ions to the left whose permeabilities are more sensitive to differences in hydration energy than the ions to the right that are less sensitive. The permeability of ions having hydration energies greater than Cl fall off very quickly with increases in ΔG_{hyd}: over a range of ~50 kJ/mol, the permeabilities fall by an order of magnitude. In contrast, the permeabilities of anions having hydration energies less than Cl are considerably less sensitive to hydration energy: P_x/P_{Cl} increases an order of magnitude over ~150 kJ/mol.

Fig. 6 D also suggests the possibility that the diameter of the channel pore may be very large. Although on the log scale it appears that P_x/P_{Cl} is approaching a plateau, there is no evidence for any decrease in P_x/P_{Cl} with increases in anion radius. The most permeant an-

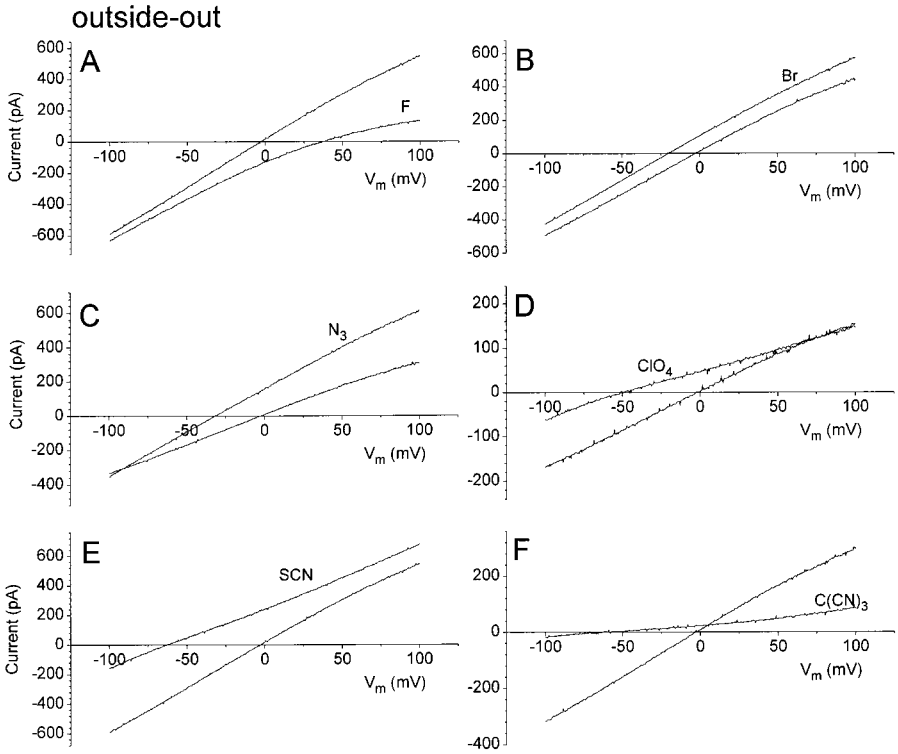

FIGURE 4. I–V relationships of $I_{Cl,Ca}$ in outside-out patches with different external anions. The conditions were the same as Fig. 2, except that the patch was outside-out. (A) Fluoride; (B) bromide; (C) azide; (D) perchlorate; (E) thiocyanate; and (F) tricyanomethanide.

ion, $C(CN)_3$, is also the largest we have tested. The estimated equivalent radius of this molecule is 0.304 nm. Thus, this channel is relatively large, with a pore diameter exceeding 0.6 nm. Because we have not tested any anions that have both smaller hydration energies and larger radii than $C(CN)_3$, the possibility exists that the pore diameter may be considerably larger than 0.6 nm.

Channel Block by Permeant Anions

Many anion channels are blocked by permeant anions. To examine the ability of substitute anions to block Cl permeation, we compared the currents in both outside-out and inside-out patches exposed to mixtures of Cl and other anions on either the external or cytoplasmic side. We concentrated our studies on ions that had a high affinity for the channel as determined above (Fig. 3 C).

Tricyanomethanide. We first examined the effect of the ion with the highest estimated permeability and affinity for the $Cl_{Ca}C$, $C(CN)_3$ (Fig. 7). The solution bathing the extracellular side of an outside-out patch was changed in steps from 100 mol% Cl to 100 mol% $C(CN)_3$. At the end of the experiment, the patch was returned to 100 mol% Cl to verify that the effect of $C(CN)_3$ was reversible. Patches in which there was a significant change in current amplitude or E_{rev} in 100 mol% Cl during the course of the experiment were discarded. The patch was also exposed to solution in which Cl was replaced with SO_4 to establish that the current was a Cl current and was not due to leak. Fig. 7 A shows the I–V curves in response to voltage ramps from −100 to +100 mV. Replacement of Cl with $C(CN)_3$ shifted the E_{rev} in a negative direction and reduced the conductance in both inward and outward directions. To illustrate more clearly the effect of $C(CN)_3$ on conductance, Fig. 7 B plots the current versus the driving force ($V_m - E_{rev}$) for each fractional $C(CN)_3$ replacement. Replacement of as little as 0.1 mol% Cl with $C(CN)_3$ had measurable inhibitory effects on the current. To quantify the effects of $C(CN)_3$, we measured the current at +80 and −80 mV of driving force and plotted the relative current versus mol% $C(CN)_3$ (Fig. 7 F, squares). At both positive and negative voltages, the current decreased monotonically with increasing $[C(CN)_3]$, but the IC_{50}s for current inhibition were very different at positive and negative voltages: the IC_{50} at +80 mV was ~0.3 mM, whereas at negative voltages, the IC_{50} was >10 times larger (3.6 mM). Thus, $C(CN)_3$ blocks the channel most potently when it is drawn into the channel from the extracellular side. The increase in IC_{50} at negative potentials can be explained as relief of block as $C(CN)_3$ is drawn out of the channel.

To understand more thoroughly the voltage dependence of the effect of $C(CN)_3$, the currents in Fig. 7 B were expressed as a fraction of the current in 100 mol% Cl ($I_{C(CN)3\,=\,0}$) (Fig. 7 C). Relative current amplitude decreased with depolarization, showing that inhibition of the current by $C(CN)_3$ was voltage-dependent. Increasing the mol% $C(CN)_3$ increased the amount of block of the current and increased the cur-

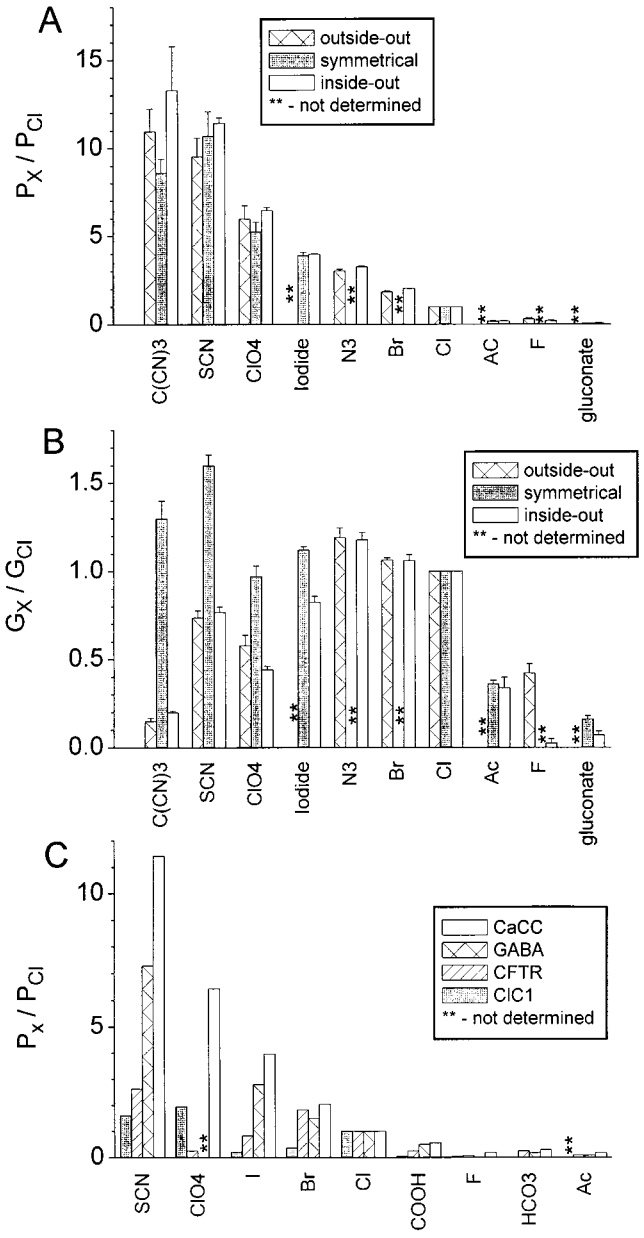

FIGURE 5. Comparison of permeabilities and conductances. (A) Relative permeabilities. (B) Relative conductances. (Open bars) Inside-out patches with changes in cytoplasmic solution (n = 3–5). (Cross-hatched bars) Outside-out patches with changes in external solution (n = 3–4). (Closed bars) Inside-out patches with substitute anion on both sides of the membrane was compared with Cl on the cytoplasmic side (n = 3–6). (C) Comparison of P_x/P_{Cl} in different anion channels. $Cl_{Ca}C$ (open bars; data from this paper); $GABA_A$ receptor (cross-hatched bars; data from Bormann et al., 1987); CFTR (slant-hatched bars; data from Linsdell and Hanrahan, 1998); and ClC-1 (closed bar; data from Rychkov et al., 1998).

vature of the plot. The data in Fig. 7 C were replotted in Fig. 7 D for each voltage as a function of the mol% $C(CN)_3$. These data were fitted to an equation of the form $I/I_{C(CN)3\,=\,0} = I_{min} + \{(I_{max} - I_{min}) / 1 + ([C(CN)_3] / K_d)^n\}$, where I_{max} and I_{min} are maximum and minimum current amplitudes, K_d is the concentration of $C(CN)_3$ required to reduce the current to a value equal to $(I_{max} - I_{min})/2$, and n is the slope factor. The concentration of $C(CN)_3$ required to reduce the current to a value equal to $(I_{max} - I_{min})/2$ for each voltage was derived from these plots. Fig. 7 E is a plot of the average K_d versus voltage obtained from four experiments. The apparent K_d of $C(CN)_3$ block was voltage-dependent. The minimum K_d ($\sim$ 0.4 μM) was observed between 0 mV and +90 mV. The K_d became about 10 times larger at −90 mV. From the plot of K_d versus $V_m - E_{rev}$, one can calculate the approximate fraction of the voltage field experienced by the blocking ion at its binding site using Eq. 4 developed by Woodhull (Woodhull, 1973; Hille, 1992).

$$\log K_d(V) = \log K_d(0\text{mV}) - (z\delta FV/2.303\,RT), \quad (4)$$

where $K_d(V)$ is the K_d at each voltage, $K_d(0$ mV) is the K_d at 0 mV, z is the electronic charge of the ion, and δ is the fraction of the voltage field sensed by the ion. The solid line in Fig. 7 E is the best fit of the antilog of Eq. 4 to the data. δ was estimated to be ~0.4 the distance across the voltage field from the extracellular side. Similar estimates were obtained by fitting the data in Fig. 7 C to a more general equation (see Eq. 5) derived by Woodhull (1973) to model the blocking of Na channels by protons. In Eq. 5, below, $[X]_o$ and $[X]_i$ are the concentrations of blocking ion X inside and outside the membrane, A is the relative rate constant for ions returning to the extracellular space relative to their rate of entering the blocking site, and C is the relative rate constant for ions entering the site from the cytosolic side.

This model assumes that the blocking ion binds to an energy well within the pore of the channel, and that entry and exit of the blocking ion are determined by barriers on the cytoplasmic and extracellular sides. The thin lines in Fig. 7 C are the best fits of the data to Eq. 5. Although the fits are not perfect, they sufficiently approximate the data to suggest that a two-barrier, one-well model is a reasonable starting point. The δ estimated from these fits was 0.4 ± 0.02, which agrees with the estimate from Fig. 7 E.

We also examined the effect of cytoplasmic $C(CN)_3$ on the current and obtained quantitatively different re-

$$I/I_{C(CN)3\,=\,0} = \frac{A \cdot \exp(z\delta FV/RT) + (C \cdot A) \cdot \exp[z(2\delta - 1)FV/2RT]}{[X]_o + [X]_i \cdot C \cdot \exp(zFV/2RT) + A \cdot \exp(z\delta FV/RT) + (C \cdot A) \cdot \exp[z(2\delta - 1)FV/2RT]} \quad (5)$$

sults (Fig. 7, G-L). First, the current was much less sensitive to $C(CN)_3$ block from the inside than from the outside. The IC_{50} for cytoplasmic $C(CN)_3$ block at −80 mV was at least 15 times larger than the IC_{50} for external $C(CN)_3$ block at +80 mV (Fig. 7 F). Second, the voltage dependence of $C(CN)_3$ block from the cytoplasmic side was less pronounced than for the $C(CN)_3$ block from the extracellular side: the K_d for cytoplasmic $C(CN)_3$ changed only ~2-fold between 0 to −100 mV compared with an ~10-fold change for extracellular $C(CN)_3$. It was not possible to fit the data in Fig. 7 I to Eq. 5 over the entire voltage range. However, estimates of δ obtained by fitting the data in Fig. 7 L to Eq. 4 were 0.6 for negative potentials and 0.5 for positive potentials. These data show that the $Cl_{Ca}C$ behaves asymmetrically with regard to block by permeant anions and that there is one or possibly two blocking sites near the middle of the voltage field.

Thiocyanate. We next examined the effect of SCN, which has been used extensively in studying anion channel permeation. From Fig. 3 C, we predict that SCN has about a 4.5-fold lower affinity for the channel than $C(CN)_3$. Fig. 8 (A–E) shows the data for an outside-out patch with external SCN and Fig. 8 (F–J) shows data for an inside-out patch with cytoplasmic SCN. The blocking effect of SCN on the conductance was considerably less than the effect of $C(CN)_3$ (Fig. 8, B and H). The maximum inhibition of the current by SCN was only ~40% in both the inside-out and outside-out configurations (Fig. 8, C and I). SCN was clearly more conductive than $C(CN)_3$ and did not block the Cl current as completely as $C(CN)_3$. Despite the less robust inhibition, we analyzed the SCN block in the same way we analyzed the $C(CN)_3$ block. The plots of relative current versus mol% SCN (Fig. 8, D, E, J, and K) were fit to the equation $I/I_{SCN=0} = I_{min} + \{(I_{max} - I_{min}) / 1 + ([SCN] / K_d)^n\}$. The K_ds, defined as the concentration of SCN required to block the current half-maximally, were plotted versus $V_m - E_{rev}$ (Fig. 8, F and L). The current was more sensitive to block by extracellular SCN than cytoplasmic SCN: the K_ds at 0 mV were 1.7 mM for external SCN and 3.6 mM for internal SCN. Block by SCN from the outside was not strongly voltage-sensitive. When applied from the outside, the affinity of SCN for the channel at 0 mv was about four times less than the affinity of $C(CN)_3$.

Anomalous Mole Fraction Behavior

Many ion channels exhibit anomalous mole fraction behavior: the conductance of a mixture of two permeant ions is different than one would predict from

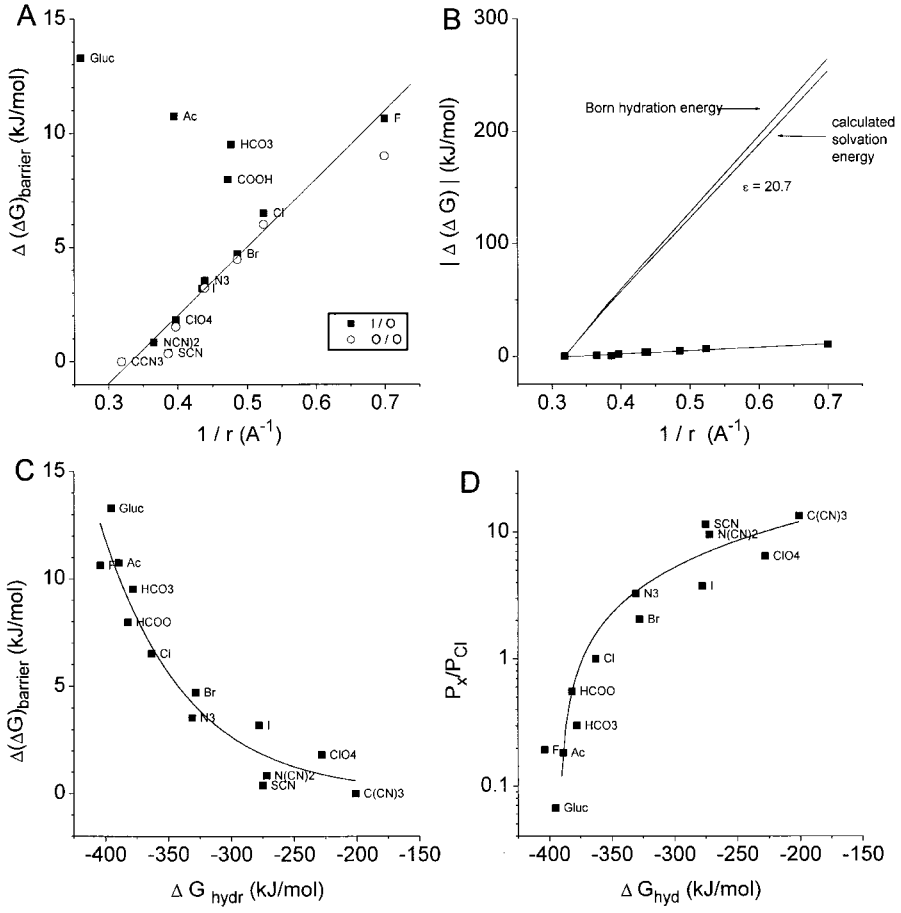

FIGURE 6. Analysis of anion permeation through $Cl_{Ca}C$ channels. (A) The relative energy barrier height ($\Delta(\Delta G)_{barrier}$) was calculated from the permeabilities relative to $C(CN)_3$ in Fig. 5 using Eq. 2. $\Delta(\Delta G)_{barrier}$ was plotted versus the reciprocal of the ionic radius of the anion after applying the Lattimer correction (Smith et al., 1999). (Closed squares) Inside-out patches; (open circles) outside-out patches. The line is the best fit to the data points excluding gluconate, acetate, bicarbonate, and formate. (B) Calculation of the effective dielectric constant of the pore. The relative Born hydration energy in water (heavy solid line) was calculated from Eq. 3 with $\varepsilon = 80$ (water). The line ($\Delta(\Delta G)_{barrier}$) through the data points is from A. Relative solvation energy (thin line) was calculated by subtracting the fit to the data points from the heavy line. (C) $\Delta(\Delta G)_{barrier}$ versus measured free energies of hydration. Hydration free energies were obtained from Marcus (1997) or were extrapolated from potentiometric measurements (Smith et al., 1999). (D) Relative permeabilities versus hydration free energy.

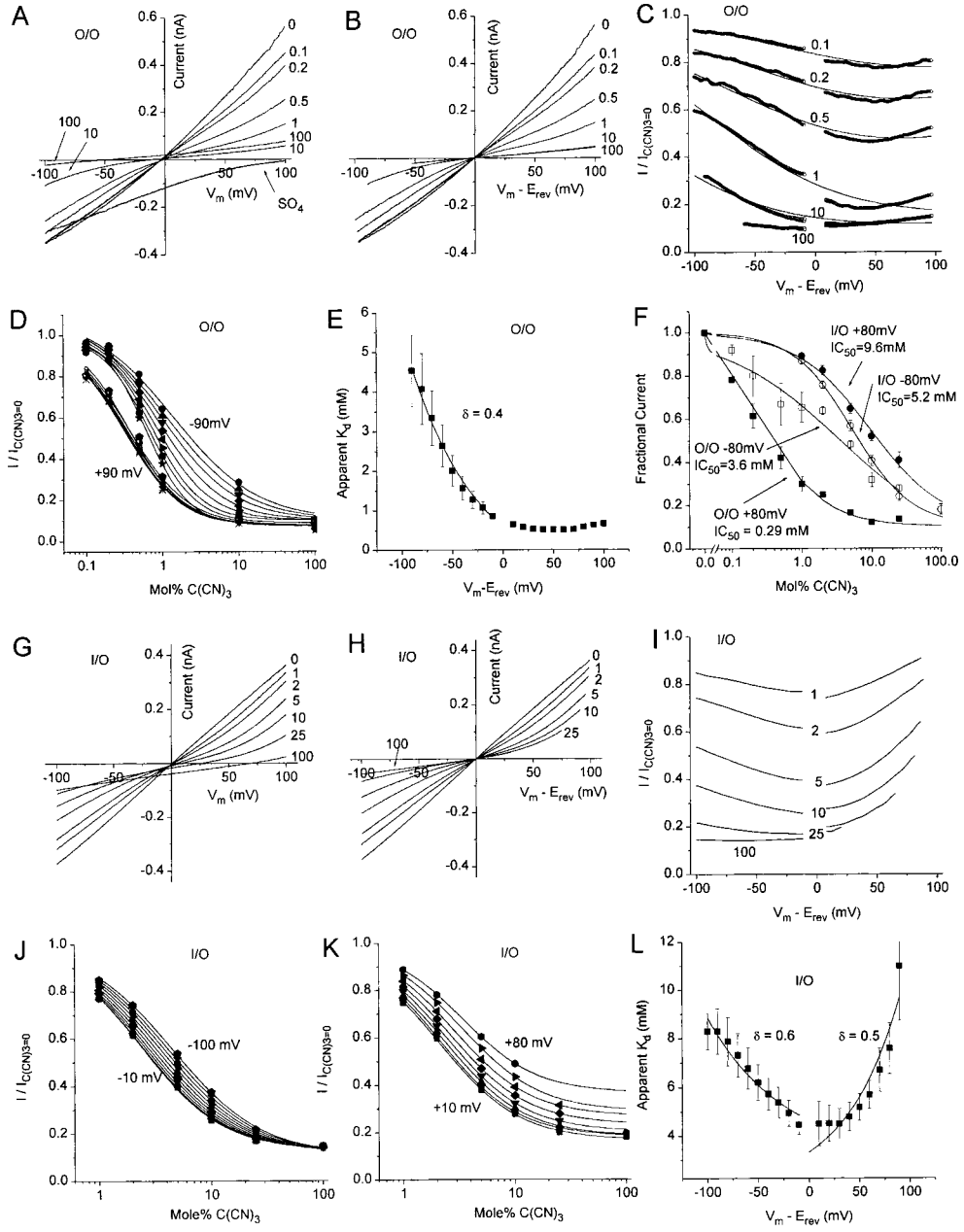

FIGURE 7. $I_{Cl.Ca}$ block by $C(CN)_3$. (A–E) Outside-out patch with $C(CN)_3$ on the extracellular face. (G–L) Inside-out patch with $C(CN)_3$ on the cytoplasmic side. The bath solutions contained 10 mM TES, pH 7.2, 0.1 mM $CaCl_2$, and 150-mM mixtures of NaCl and $KC(CN)_3$. The pipet contained the same solution with 150 mM NaCl. The patch was voltage-clamped with a 250-ms duration voltage ramp from −100 to +100 mV. (A) I–V relationships in outside-out patches with the following external mol% $C(CN)_3$ (the balance being Cl) as marked: 0, 0.1, 0.2, 0.5, 1, 10, and 100. The line marked "SO_4" is the I–V curve obtained with Cl replaced with SO_4 on the external side to evaluate leak. (B) The I–V curves in A were replotted versus the driving force ($V_m - E_{rev}$) for each anion mixture. (C) Voltage-dependent block of $I_{Cl.Ca}$ by $C(CN)_3$. (Heavy lines) Each curve in B was divided by the curve obtained in 100 mol% Cl. (Light lines) Fit of the data to Eq. 5 (see text). (D) Concentration- and voltage-dependent block of $I_{Cl.Ca}$. The data in C were replotted for various potentials as a function of mol% $C(CN)_3$. The data were fitted to the logistic equation: $I/I_{C(CN)3\,=\,0} = I_{min} + \{(I_{max} - I_{min}) / 1 + ([C(CN)_3] / K_d)^n\}$ (solid lines). (E) Apparent K_d of extracellular $C(CN)_3$ as a function of voltage. The apparent K_d at each voltage was determined from the fits in D in four separate experiments and averaged. (F) Inhibition of the current in both inside-out and outside-out patches as a function of mol% $C(CN)_3$. The current was measured at +80 and −80 mV of driving force. The current relative to that in 100% Cl was plotted versus $[C(CN)_3]$. (Squares) Outside-out patches; (circles) inside-out patches; (open symbols) −80 mV; and (closed symbols) +80 mV. (G) I–V relationships for inside-out patches with the following cytoplasmic mol% $C(CN)_3$ (the balance being Cl) as marked: 0, 1, 2, 5, 10, 25, and 100. (H) The I–V curves in G were replotted versus the driving force ($V_m - E_{rev}$) for each anion mixture. (I) Voltage-dependent block of $I_{Cl.Ca}$ by $C(CN)_3$. Each curve in H was divided by the curve obtained in 100 mol% Cl. (J and K) Concentration- and voltage-dependent block of $I_{Cl.Ca}$. The data in I were replotted for various potentials as a function of mol% $C(CN)_3$. The data were fitted to the logistic equation (solid lines). (L) Apparent K_d of cytoplasmic $C(CN)_3$ as a function of voltage. The apparent K_d at each voltage was determined from the fits in J and K for four separate experiments and averaged.

the independent behavior of the pure ions separately. This behavior is often explained by a single-file channel occupied by two or more ions that interact within the pore (see Hille, 1992; Nonner et al., 1998 for references). Anomalous mole fraction effects have been reported by some (but not all) investigators for CFTR and ClC-1 (see Fahlke et al., 1997a; Dawson et al., 1999 for references and discussion). In this section, we discuss the evidence for anomalous mole fraction behavior of the $Cl_{Ca}C$.

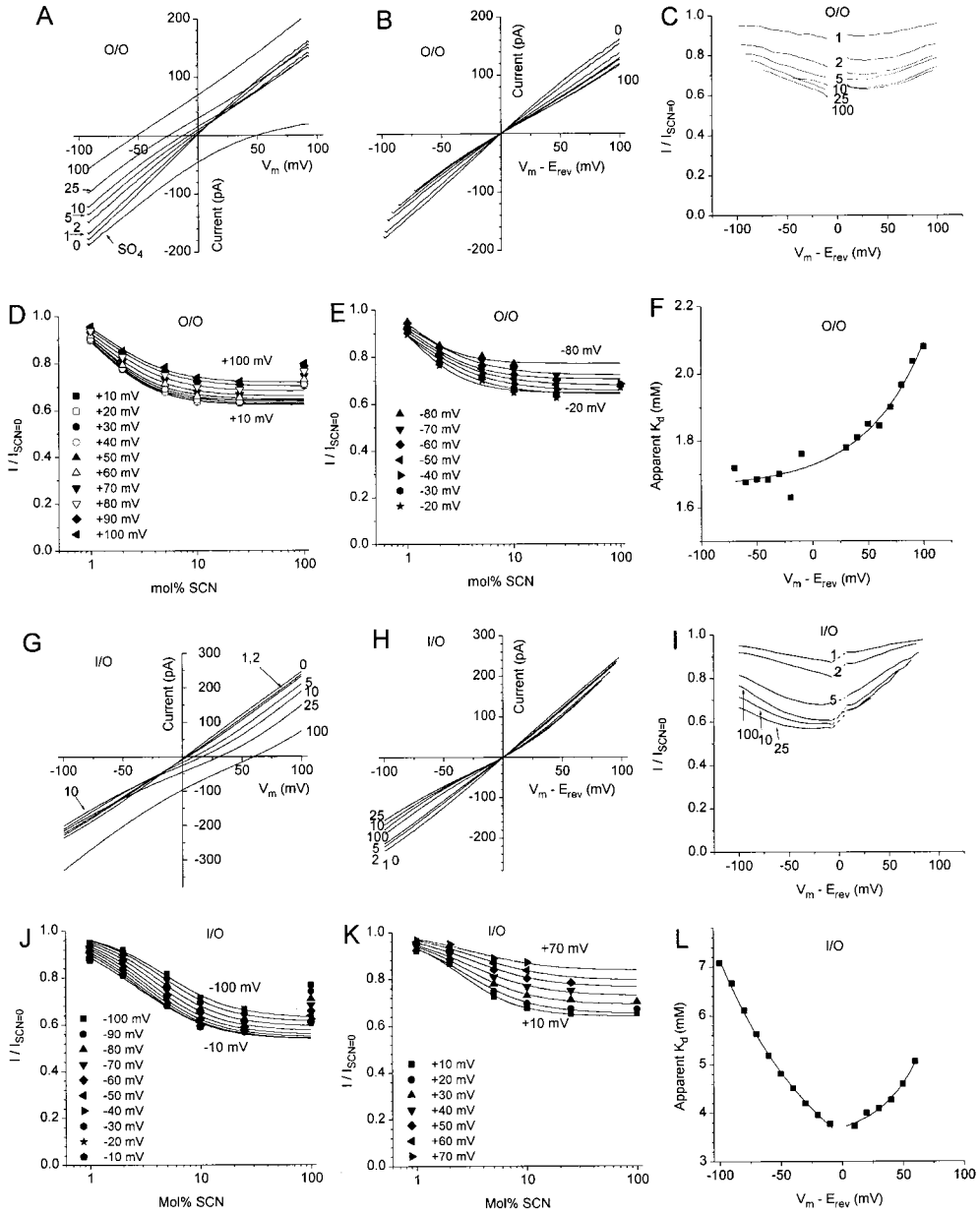

FIGURE 8. $I_{Cl.Ca}$ block by SCN. (A–F) Outside-out patch with SCN on the extracellular face. (G–L) Inside-out patch with SCN on the cytoplasmic side. Bath solutions contained 10 mM TES pH 7.2, 0.1 mM $CaCl_2$, and 150-mM mixtures of NaCl and NaSCN. The pipet contained the same solution with 150 mM NaCl. The patch was voltage-clamped with a 250-ms duration voltage ramp from −100 to +100 mV. (A) I–V relationships with the following external mol% SCN (the balance being Cl) as marked: 0, 1, 2, 5, 10, 25, and 100. (B) The I–V curves in A were replotted versus the driving force ($V_m - E_{rev}$) for each anion mixture. (C) Voltage-dependent block of $I_{Cl.Ca}$ by external SCN. Each curve in B was divided by the curve obtained in 100 mol% Cl. (D and E) Concentration- and voltage-dependent block of $I_{Cl.Ca}$. The data in C were replotted for various potentials as a function of mol% SCN. The data were fitted to the logistic equation (solid lines). In D, the data points at 100 mol% SCN were ignored in fitting the curves. This experiment is representative of three experiments. (F) Apparent K_d of extracellular SCN as a function of voltage. The apparent K_d at each voltage was determined from the fits in D and E. (G) I–V relationships with the following cytoplasmic mol% SCN (the balance being Cl) as marked: 0, 1, 2, 5, 10, 25, and 100. (H) The I–V curves in G were replotted versus the driving force ($V_m - E_{rev}$) for each anion mixture. (I) Voltage-dependent block of $I_{Cl.Ca}$ by cytoplasmic SCN. Each curve in H was divided by the curve obtained in 100 mol% Cl. (J and K) Concentration- and voltage-dependent block of $I_{Cl.Ca}$. The data in I were replotted for various potentials as a function of mol% SCN. The data were fitted to the logistic equation (solid lines). In J, the data points at 100 mol% SCN were ignored in fitting the curves. This experiment is representative of five experiments. (L) Apparent K_d of cytoplasmic SCN as a function of voltage. The apparent K_d at each voltage was determined from the fits in J and K.

We consistently observed that in inside-out patches with cytoplasmic SCN, the current was blocked more by 25 mol% SCN than by 100 mol% SCN (Fig. 8 H). This nonlinear relationship between block and substitute anion concentration was also revealed in plots of relative current versus mol% SCN (Fig. 8, D and J), where the relative current at 100 mol% SCN was greater than at 25 mol% SCN. This behavior was suggestive of anomalous mole fraction behavior, but because the channel only showed this behavior with SCN and not with $C(CN)_3$, it remained unclear whether this provided evidence for a multi-ion pore. Fig. 9 examines the multi-ion properties of the channel in more detail. E_{rev} does not show prominent anomalous mole fraction behavior. The E_{rev}s of the I–V curves were shifted in a negative direction with increasing mol% SCN or $C(CN)_3$, as shown in Figs. 7 and 8. The shift in E_{rev} with SCN coincided very closely with that predicted by the GHK equa-

tion (Fig. 9 A, open circles). However, the shift in E_{rev} with $C(CN)_3$ could not be fit well by the GHK equation (Fig. 9 A, closed squares): the change in E_{rev} with small mol% $C(CN)_3$ was less than that predicted from the shift in E_{rev} at 100 mol% $C(CN)_3$. Calculation of the P_x/P_{Cl} ratios from the shifts in E_{rev} at different mol% substitute anions are shown in Fig. 9 B. For SCN, the calculated P_{SCN}/P_{Cl} ratio was relatively independent of the mol% SCN. However, with $C(CN)_3$, the $P_{C(CN)3}/P_{Cl}$ ratio increased from 4 at 1 mol% $C(CN)_3$ to 8.8 at 100 mol% $C(CN)_3$. This is suggestive of anomalous mole fraction behavior (Hille, 1992). The reader may notice that this $P_{C(CN)3}/P_{Cl}$ ratio was slightly smaller than what we reported in Fig. 3. These two sets of data were obtained from different patches and the difference may reflect the age of the $C(CN)_3$ solutions (see MATERIALS AND METHODS).

Additional evidence of anomalous mole fraction behavior was observed when we measured the slope conductance as a function of mol% SCN. The slope conductance was calculated as $(I_{DF} - I_{DF-20})/20$ mV, where I_{DF} is the current at each driving force ($DF = V_m - E_{rev}$) and I_{DF-20} is the current at a potential 20 mV less (Fig. 9 C). The slope conductance at various potentials was plotted versus mol% SCN (Fig. 9 D). At negative potentials, the slope conductance reached a minimum between 10 and 25 mol% SCN, and then increased at greater mol% SCN. The minimum in the slope conductance also suggested anomalous mole fraction behavior.

Effects of Different Anions on $I_{Cl,Ca}$ at Low [Ca^{2+}]

All experiments above used a concentration of Ca^{2+} (100 μM) that maximally activated the $Cl_{Ca}C$ channels. In an earlier study, we observed that the activation of the currents at low [Ca^{2+}] seemed faster with I and Br than with Cl (Kuruma and Hartzell, 2000). To investigate this more closely, we compared the currents at [Ca^{2+}] between 10^{-7} and 10^{-6} M with symmetrical Cl and with cytoplasmic Cl replaced with SCN (Figs. 10 and 11). Ca^{2+} concentrations were confirmed by Fura-2 measurements.

Fig. 10 shows currents at several different [Ca^{2+}] with cytoplasmic Cl and SCN. There are several obvious differences between the Cl and SCN traces. First, at comparable [Ca^{2+}], the outward currents with cytoplasmic Cl activated more slowly than those with cytoplasmic SCN. Second, at comparable [Ca^{2+}] at the same voltage, the steady state inward currents and the ratio of inward and outward currents at steady state with cytoplasmic Cl were smaller than those with SCN.

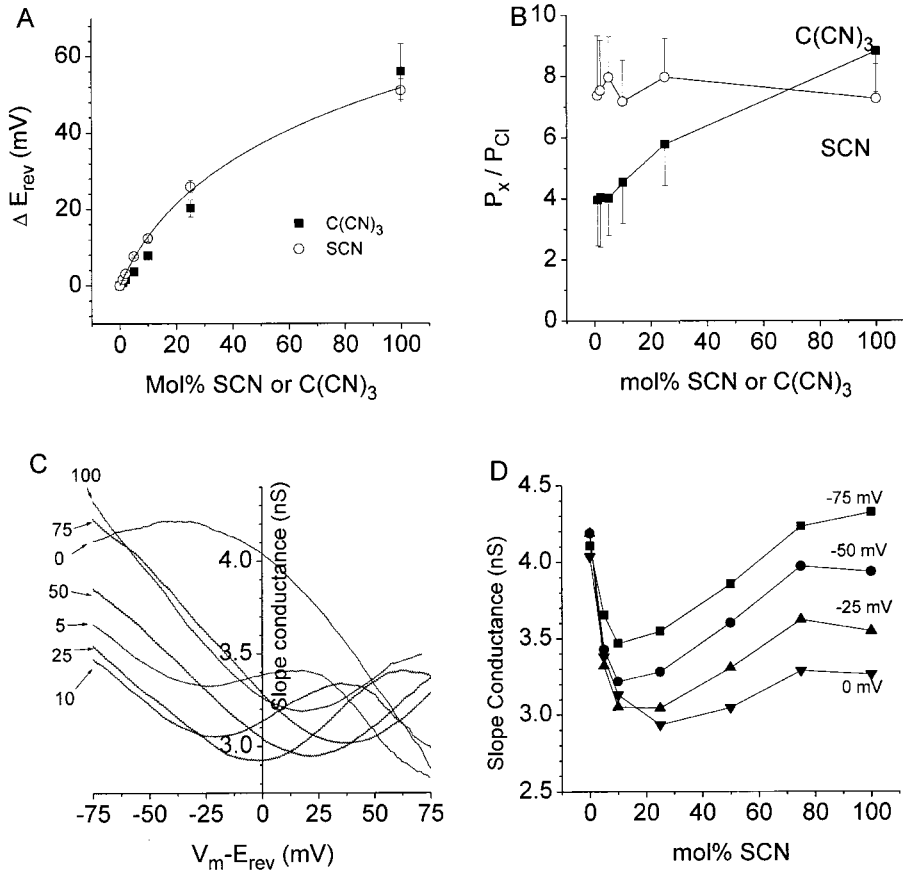

FIGURE 9. Anomalous mole fraction behavior of $Cl_{Ca}Cs$. (A) Dependence of E_{rev} on mol% $C(CN)_3$ or SCN. The E_{rev}s corrected for liquid junction potential obtained from experiments such as those in Figs. 7 and 8 were plotted versus mol% of the substitute anion. (Open symbols) SCN, $n = 5$; (closed symbols) $C(CN)_3$, $n = 4$. (Solid line) Goldman-Hodgkin-Katz equation with $P_{SCN}/P_{Cl} = 8$. (B) Dependence of permeability ratio on mol% of SCN or $C(CN)_3$. P_x/P_{Cl} was calculated from the data in A from the form of the Goldman-Hodgkin-Katz equation: $P_x/P_{Cl} = [Cl_o \cdot (\exp(F/RT \cdot \Delta E_{rev}) - 1) / X_i] + 1$, where $Cl_o = 150$ mM and X_i is the concentration of the substitute anion. (C) Dependence of slope conductance on driving force at different mol% SCN. The slope conductance was determined by calculating the slope of the I–V curve of an inside-out patch like the one in Fig. 8 using a 20-mV moving window. The resulting curves were smoothed by the FFT smoothing algorithm in Origin and the slope conductance was plotted versus the driving force for different mol% SCN (labels to left of curves). (D) Slope conductance versus mol% SCN. The slope conductance for four different voltages in C was plotted versus mol% SCN. The curves show a minimum slope conductance at 10–25 mol% SCN.

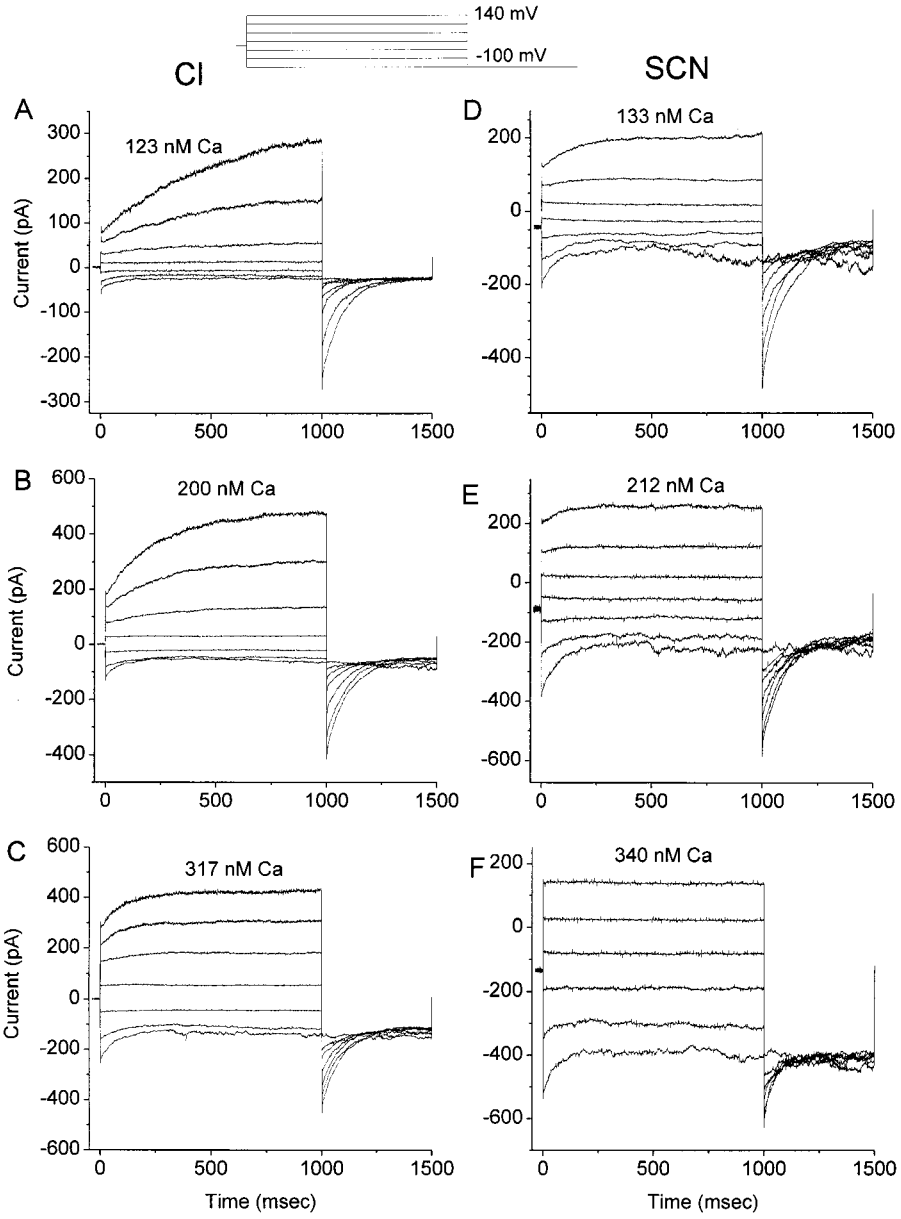

FIGURE 10. Current traces of $I_{Cl.Ca}$ in low free [Ca^{2+}] with Cl or SCN as permeant anion. All traces are from the same patch. Inside-out excised patches were voltage-clamped in symmetrical 150 mM NaCl (A–C) or with 150 mM NaSCN on the cytoplasmic side and 150 mM NaCl on the external side (D–F). The solutions also contained 10 mM TES, pH 7.2, and 10 mM EGTA plus Ca-EGTA, as described in MATERIALS AND METHODS, to adjust the free [Ca^{2+}] to the concentrations indicated on the cytoplasmic side. Ca^{2+} concentrations were measured by Fura-2 fluorescence. The patches were clamped from a holding potential of 0 mV to potentials between +140 and −100 mV for 1 s, followed by a 500-ms pulse to −100 mV. These traces are typical of four experiments.

Fig. 11 A plots the instantaneous tail currents measured at −100 mV as a function of the preceding voltage step. The curves for SCN are considerably above those for Cl. For example, the curve for SCN in 133 nM Ca^{2+} was located above the curve for Cl in 200 nM Ca^{2+}. The E_{rev} in SCN was 58 mV positive to that in Cl, so the data were replotted as conductance versus driving force in Fig. 11 B. The difference between Cl and SCN remains evident in this plot. The conductance versus [Ca^{2+}] was then plotted for Cl (Fig. 11 C) and SCN (Fig. 11 D), and the data were fitted to the Hill equation. Fig. 11 E plots the apparent K_d derived from Hill fits as a function of voltage for Cl and SCN. The apparent K_d of the channel for Ca^{2+} in the presence of SCN is smaller than in the presence of Cl. The K_d for Ca^{2+} in Cl at 0 mV was 279 nM, whereas in SCN, it was ~50% as large, 131 nM. This result suggests that the presence of the permeant anion in the pore affects the binding of Ca^{2+}. The K_d exhibits approximately the same voltage dependence for both anions.

When we fit the data in Fig. 11 (C and D) to the Hill equation, G_{max} was fixed to the same value for all potentials (see figure legend). We felt it was justified to fit the data from all potentials to the same G_{max} because our previous, more extensive study on the voltage dependence of $I_{Cl.Ca}$ showed that G_{max} at maximum [Ca^{2+}] at different potentials was the same (Kuruma and Hartzell, 2000). We were limited in the number of [Ca^{2+}] we could test in the same patch because of rundown of $I_{Cl.Ca}$ in excised patches (Kuruma and Hartzell, 2000). Unfortunately, this limited the number of data points we had available for fitting. It should be noted that the K_ds determined from the experiments with Cl in Fig. 11 were smaller than those we published previously (Ku-

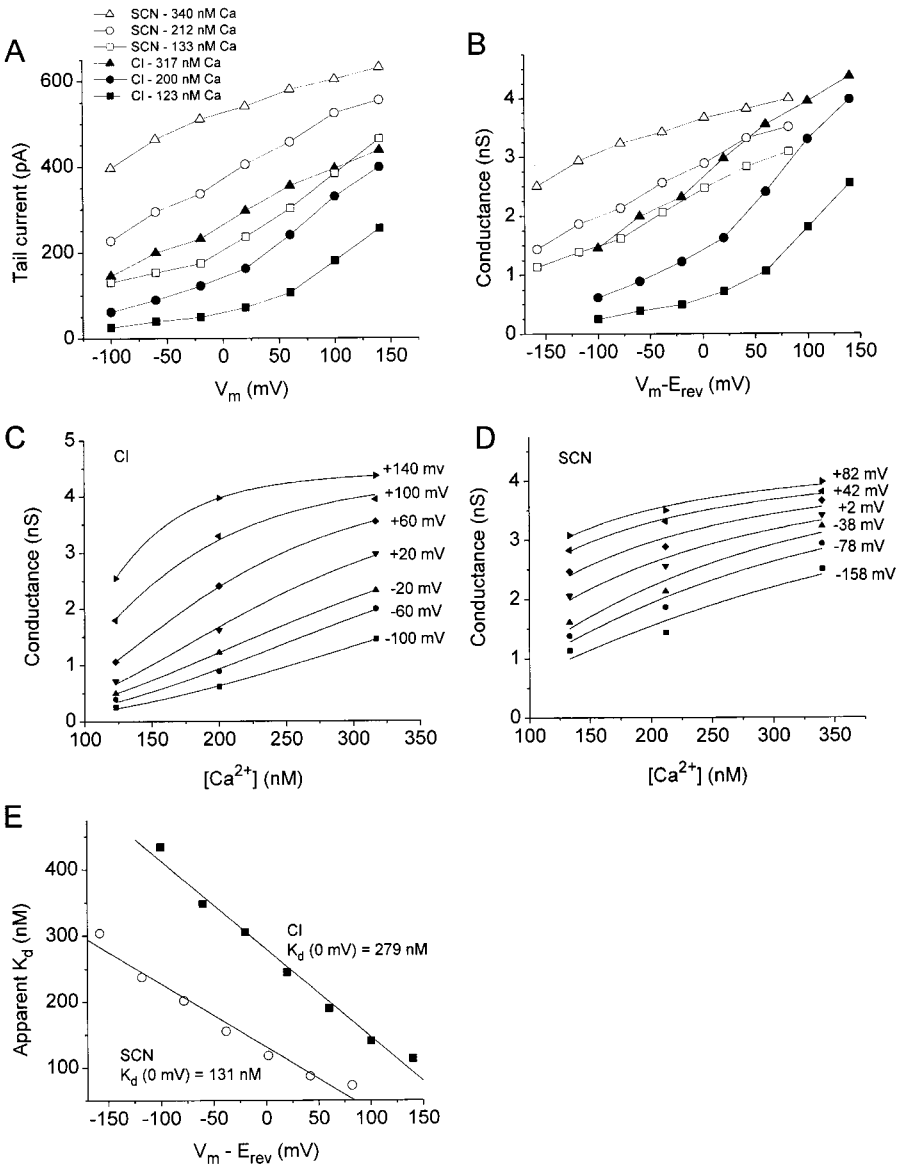

FIGURE 11. Calcium dependence of $I_{Cl.Ca}$ with Cl or SCN as permeant anion. (A) Tail currents versus voltage. The instantaneous tail currents at –100 mV in Fig. 10 were plotted versus voltage for each condition (open symbols, SCN; closed symbols, Cl; [Ca^{2+}] as indicated). (B) Conductance versus voltage. The conductance of the traces in Fig. 10 was determined by measuring the amplitudes of the instantaneous tail currents at −100 mV and dividing by the driving force ($V_m - E_{rev}$). E_{rev} was shifted +58 mV in SCN compared with Cl. (C) Conductance versus free [Ca^{2+}] at various potentials with Cl as permeant anion. The data were fitted to the Boltzmann equation: $G = G_{min} - [(G_{max} - G_{min}) / 1 + e^{([Ca]-K_d)/s}]$, where G_{max} and G_{min} are the maximum and minimum conductances, respectively, and s is the slope factor. G_{max} was fixed at 4.46 nS for Cl and 4.54 nS for SCN, and G_{min} was fixed at 0. G_{max} was chosen by preliminary fitting sessions using the data from the most positive potentials and allowing all variables to float. Our previous extensive study on the voltage dependence of $I_{Cl.Ca}$ (Kuruma and Hartzell, 2000) justified using the same G_{max} for all voltages. Because of problems with rundown of $I_{Cl.Ca}$ in excised patches (Kuruma and Hartzell, 2000), we were able to test only a limited number of [Ca^{2+}] before rundown exceeded 10%. This limited the number of data points we had available for fitting. (D) Conductance versus free [Ca^{2+}] at various potentials with SCN as the permeant anion. (E) Apparent K_d for Ca^{2+} is different in the presence of Cl and SCN. The apparent K_d was extracted from the Boltzmann fits in C and D and plotted versus membrane potential. These data are typical of four experiments.

ruma and Hartzell, 2000). This difference is due to the absence of Mg^{2+} in our solutions in the present experiments. We have found that Mg^{2+} decreases the apparent affinity for Ca^{2+} (Hartzell, C., and Z. Qu, unpublished observations). In the patches analyzed, rundown did not exceed 10% over the course of the experiment.

Effect of Internal and External pH on Cl^- Permeation

We observed that the rectification of the current depended on pH. To investigate this more carefully, we exposed the cytoplasmic face of excised patches to solutions having pH adjusted between pH 7.0 and 9.5 with HEPES-NaOH. An example of a typical patch is shown in Fig. 12 A. As cytoplasmic pH was increased, the inward current was reduced, while the outward current was not significantly affected (Fig. 12, B and C). To quantify the effect of pH, we calculated the amplitude of the current at a different pH as a fraction of the current at pH 7 ($I/I_{pH\,7}$), and plotted this as a function of V_m (Fig. 12 D). The effect of pH was clearly voltage-dependent, with the maximum inhibition occurring at negative potentials. These data are replotted in Fig. 12 E, where I/I_{pH7} is plotted versus the pH for different potentials. The data were fit to the Hill equation. The

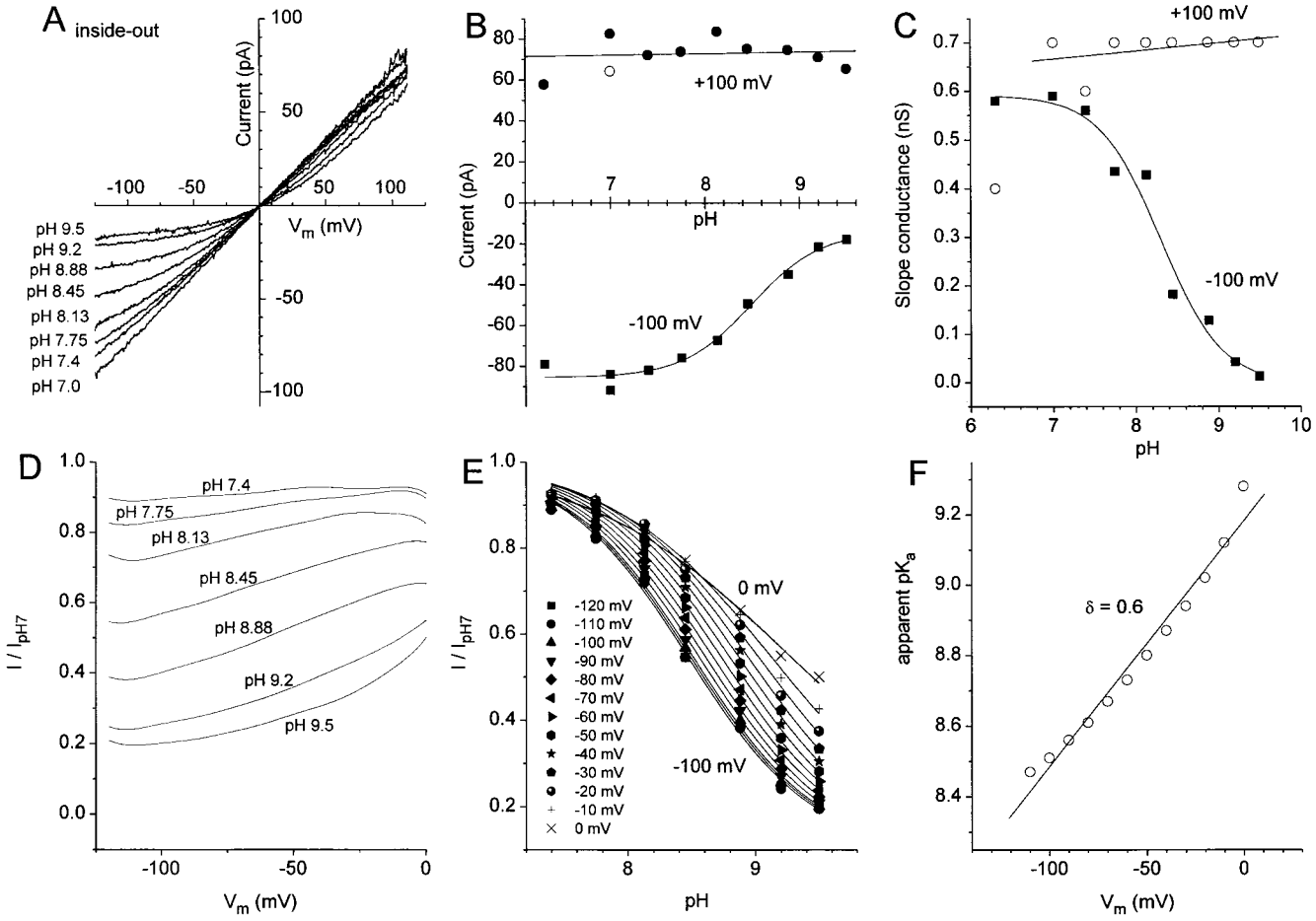

FIGURE 12. Dependence of $I_{Cl,Ca}$ on cytoplasmic pH. An inside-out patch was exposed to bath solutions composed of 150 mM NaCl, 0.1 mM $CaCl_2$, and 10 mM HEPES, adjusted to pH between 6.3 and 9.5 with NaOH. The pipet contained the same solution at pH 7.0. The patch was voltage-clamped by a ramp from −120 to +120 mV. (A) I–V relationship for pH 7.0, 7.4, 7.75, 8.13, 8.45, 8.88, 9.2, and 9.5. (B) Amplitude of the current at +100 mV (circles) and −100 mV (squares) for the traces shown in A and also pH 6.3. (C) Slope conductance measured between −100 and −120 mV (closed squares) or between +100 and +120 mV (open circles). (D) Voltage dependence of pH block. The currents at each pH in A were divided by the current at pH 7.0 and plotted versus membrane potential. (E) pH- and voltage-dependent block of $I_{Cl,Ca}$. The data in D was replotted versus pH. (F) Apparent pKa versus V_m. The apparent pKa of current block was determined from the fits to the data in E and plotted versus membrane potential. This experiment is typical of eight experiments.

apparent affinity of the current for pH block is clearly voltage-dependent, with the highest affinity at most negative V_m. The apparent pKa derived from the fits to the data in Fig. 12 E are plotted in Fig. 12 F. The apparent pKa varied approximately onefold over the 120-mV range. The data in Fig. 12 E were fit to the following equation (Woodhull, 1973; Hille, 1992):

$$\mathrm{pKa}(V) = \mathrm{pKa}(0\ \mathrm{mv}) + (z\delta FE/2.303\ RT), \qquad (6)$$

where δ is the electrical distance from the outside. If $z = 1$, the fit to these data predicts an apparent pKa at 0 mV of 9.18 and $\delta = 0.6$. There are several possible interpretations of these data. One possibility is that protons are titrating a residue in the conduction pathway that is important for permeation. Another possibility is that the channel is blocked by OH ions. A pH of 9.18 corresponds to an [OH] of 1.5×10^{-5} M. The apparent affinity of the site for OH ions at −120 mV, therefore, would be 2.5×10^{-6} M.

Because CFTR has been shown to be blocked by certain pH buffers (Tabcharani et al., 1997), we also examined the effect of pH in solutions buffered by TRIS, MES, TES, and Tricine buffers. The results were identical to those presented for HEPES in Fig. 12.

Surprisingly, the channel was also affected in a similar manner by external pH. We examined the effect of external pH in inside-out patches by comparing different patches with different pH solutions in the pipet. We also studied outside-out patches exposed sequentially to different pH solutions in the bath. The results of these two approaches were essentially identical. Fig. 13 shows the results from a typical outside-out patch. As external pH was increased, outward current decreased. The block of the current was voltage-dependent (Fig. 13, B and C)

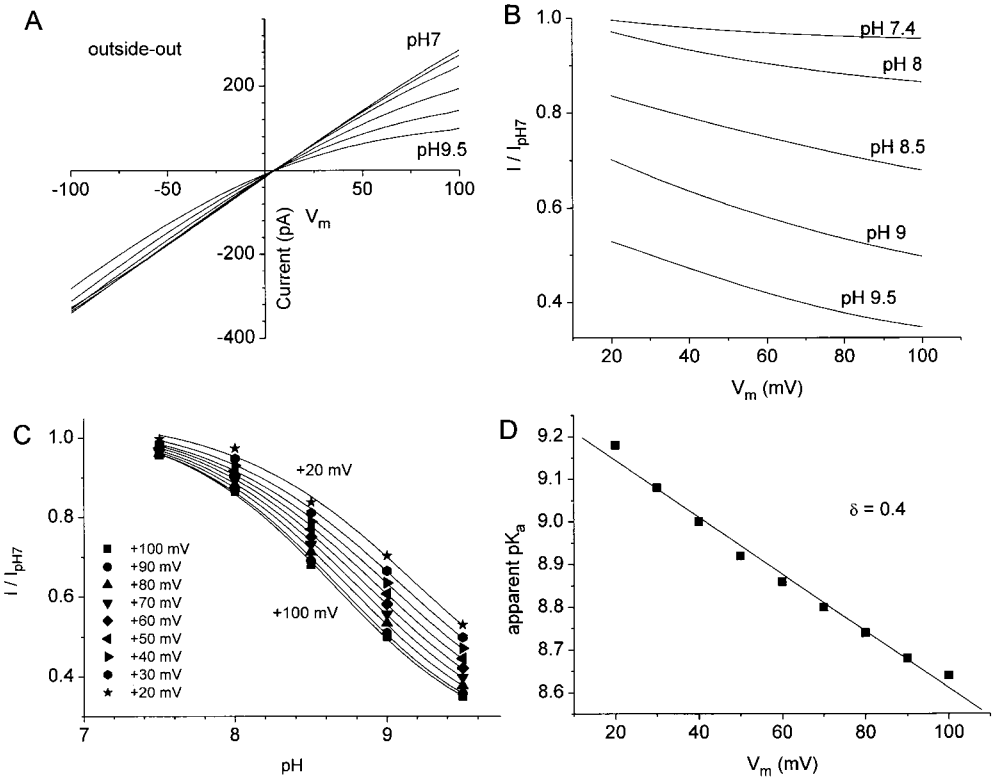

FIGURE 13. Dependence of $I_{Cl,Ca}$ on external pH. An outside-out patch was exposed to bath solutions composed of 150 mM NaCl, 0.1 mM $CaCl_2$, 10 mM HEPES, adjusted to pH between 7.0 and 9.5 with NaOH. The pipet contained the same solution at pH 7.0. The patch was voltage-clamped by a ramp from −120 to +120 mV. (A) I–V relationship for pH 7.0, 7.4, 8, 8.5, 9, and 9.5. (B) Voltage dependence of pH block. The currents at each pH in A were divided by the current at pH 7.0 and plotted versus membrane potential. (C) pH- and voltage-dependent block of $I_{Cl,Ca}$. The data in B was replotted versus pH. (D) Apparent pKa versus V_m. The apparent pKa of current block was determined from the fits to the data in C and plotted versus membrane potential. This experiment is one of two experiments in outside-out configuration and four inside-out experiments in which the solution inside the patch pipet was changed.

with the greatest block observed at positive V_m. The fit of the apparent K_d to Eq. 6 predicts an apparent pKa (0 mV) of 9.27, which is very close to that found for changes in cytosolic pH. The calculated $\delta = 0.4$. Acidic pH had little effect on the currents: current amplitudes were similar for pH between 7 and 5, although the effect of acidic solutions was not investigated systematically.

DISCUSSION

In recent years, Cl channels have received increasing attention as it has become apparent that Cl channels play fundamental roles in cell physiology. The field of Cl channel research has been advanced by the cloning of several Cl channels including CFTR, the ClC family, and ligand-gated Cl channels such as the $GABA_A$ and glycine receptor. Despite these advances, the basis of anion permeation is still much less well understood than the basis of permeation of cations through voltage-gated channels. The pore of Cl channels seems to be distributed over disparate domains of the primary sequence, unlike K channels, for example, where the pore is a highly localized structure. As our understanding of anion permeation matures, it will be necessary to have a detailed description of anion permeation in different kinds of anion channels to develop a picture of the essential structural features of an anion-selective pore. We have focused on $Cl_{Ca}Cs$ because these channels are physiologically significant in many cell types. They play roles in epithelial secretion, neuronal excitability, olfactory transduction, cardiac excitability, and fertilization. Our goal in this study was to develop a biophysical picture of anion permeation through these channels. Our findings and conclusions are summarized below.

It should be stated at the outset that because our measurements were confined to macroscopic currents, one must recognize the possibility that some of the effects we describe could be related to changes in channel gating rather than channel permeability. Our selectivity determinations, which rely on zero-current measurements, should not be subject to effects on gating, although differences in conductance with different anion species or ionic concentrations could be due, at least partly, to gating. In fact, in Fig. 10 and 11, we show that channel affinity for Ca^{2+} is about twofold different with Cl or SCN as the permeant anion, so the permeant anion clearly is able to affect channel gating. However, in all other experiments in this paper, the Ca^{2+} concentration was maintained at 100 μM, which is at least 25 times the K_d of the channel for Ca^{2+} (Kuruma and Hartzell, 2000), so it seems unlikely that a twofold effect

TABLE I

Published Permeability Ratios of Ca^{2+}-activated Cl Channels

	Skeletal muscle*	Portal vein‡	Ear artery§	Lacrimal gland‖	Epipidymal cells¶	Pulmonary artery**	T84 cell‡‡	B-TC3 cells§§	Parotid gland‖‖
SCN		14	8.3						1.8
I	3.89	4.1	4.7	2.7	2.93	2.14	2.3	3.22	1.09
NO_4	3.23	3.5	3.1	2.4	1.39			2.78	0.92
Br	1.56	2.3	2	1.6	1.33		1.45	1.59	0.75
Cl	1	1	1	1	1	1	1	1	1
F	0.11			0.05					
Acetate	0.18							0.67	
Gluconate	0.03								
SO_4	0.03				0.09				

*Hume and Thomas (1989). ‡Wang and Large (1991). §Amédéé et al. (1990). ‖Evans and Marty (1986). ¶Huang et al. (1993). **Clapp et al. (1996). ‡‡Cliff and Frizzell (1990). §§Kozak and Logothetis (1997). ‖‖Ishikawa and Cook (1993).

of the permeant anion on Ca^{2+} affinity of the channel will have a significant impact on the results. The effect of different anions on channel gating will have to await single-channel studies. However, single-channel conductances are quite small, ~2 pS (Takahashi et al., 1987), and the channels appear to flicker at relatively high frequency (Kuruma, A., and C. Hartzell, unpublished observations). Furthermore, it has been very difficult to obtain patches with only a few channels. Thus, interpretable single-channel experiments will be technically demanding. Similar problems have been encountered with other anion channels such as ClC channels that have small single-channel conductances, but analysis of macroscopic currents, as well as single-channel analysis, of both ClC and CFTR currents have provided valuable insights into channel permeation mechanisms.

Cl_{Ca}Cs Have High Relative Permeability for Large Anions

The relative permeabilities of Cl_{Ca}Cs for large anions such as SCN and $C(CN)_3$ were surprisingly large, especially compared with CFTR and ClC-1 (Fig. 5 C). For example, the P_{SCN}/P_{Cl} for Cl_{Ca}Cs was more than seven times larger than the value reported for ClC-1 (Rychkov et al., 1998) and more than three times larger than the value reported for CFTR (Linsdell and Hanrahan, 1998; Smith et al., 1999). The outwardly rectifying Cl channel in T84 cells (Halm and Frizzell, 1992) also has a low P_{SCN}/P_{Cl} compared with Cl_{Ca}Cs. These large differences in relative permeability suggest that the structure of the Cl_{Ca}C pore is different than these other channels. The ligand-gated Cl channels such as the $GABA_A$ and glycine receptors have SCN permeabilities comparable to those we found for Cl_{Ca}Cs (Bormann et al., 1987). This raises the interesting question whether Cl_{Ca}Cs may have pores more like ligand-gated Cl channels than CFTR or channels of the ClC family.

The relative permeabilities of Ca^{2+}-activated Cl channels in other tissues have been examined by other investigators. Table I summarizes these studies. The relative permeabilities of the channels from eight different tissues agree reasonably well with the values we report here for *Xenopus* oocytes. The exception is the channel from the sheep parotid gland (Ishikawa and Cook, 1993), which is altogether different than any of the others. The SCN permeabilities of rabbit ear artery and portal vein are 14 and 8.3, in close agreement with the value of 11.4 we find for *Xenopus* oocytes.

Cl_{Ca}Cs Are Permeable to Cations

The cation permeability of these channels was relatively large: $P_{Na}/P_{Cl} = 0.1$. Values for cation permeability of anion channels in the literature are quite disperse. Values for CFTR range from 0.003 to 0.2 (Tabcharani et al., 1997). Other anion channels differ significantly in their cation permeability. At least some $GABA_A$ receptors have undetectable K permeability (Bormann et al., 1987), whereas background Cl channels in the hippocampus (Franciolini and Nonner, 1987) and muscle (Blatz and Magleby, 1985) have P_{Na}/P_{Cl} ratios as high as 0.2. The explanation for this variability remains unclear, but relatively simple changes in the primary sequence can modulate cation/anion selectivities significantly. Single amino acid substitutions can increase the P_{Na}/P_{Cl} ratio in the $GABA_A$ receptor from <0.05 to >0.3 (Wang et al., 1999); the cation-selective nicotinic acetylcholine receptor can be made anion-selective by insertion of a proline residue (Galzi et al., 1992); and the glycine receptor can be made cation-selective by three point mutations in the M2 transmembrane domain (Keramidis et al., 2000).

The Pore Diameter of Cl_{Ca}Cs May Be Very Large

The Cl_{Ca}C channel appears to have a relatively large pore because ions as large as $C(CN)_3$ are highly permeable. Molecular modeling has estimated the effective radius of $C(CN)_3$ to be 0.302 nm (Smith et al., 1999).

The shape of $C(CN)_3$ is such that one dimension of the pore must be at least 0.74 nm. It seems likely that the pore diameter is actually significantly larger for several reasons. First, we have not tested anions of sufficiently large size to be excluded by the pore on the basis of size. A maximum permeability ratio has not been obtained with any of the anions tested (Fig. 6 D). We predict that anions larger than $C(CN)_3$ with low hydration energies will have high permeability ratios. Many of the larger anions used in sizing anion pores, such as gluconate, have their charge concentrated in one region of the molecule and, thus, are probably excluded from the pore not because of their physical size but because of their large hydration energies.

Second, we present evidence in Fig. 1 that the channel may be permeant to NMDG. This conclusion is based on the observation that changing NMDG concentration 10-fold does not result in the predicted 58-mV shift in the reversal potential, as would be expected if the channel were permeable exclusively to Cl. The predicted P_{NMDG}/P_{Cl} ratio was 0.06. The mean diameter of NMDG is estimated to be 0.72 nm. Thus, the possibility exists that the pore may have a diameter >7 nm. Franciolini and Nonner (1994a) have shown that a Cl channel in hippocampal neurons is permeable to large organic anions such as triethanolamine, benzyltrimethylamine, and bis-TRIS-propane. Bis-TRIS-propane has a diameter of 0.7 nm. Franciolini and Nonner (1994a,b) show that cations can only permeate in the presence of permeant anions and propose that anions and cations form mixed complexes while traversing the channel. A similar mechanism may operate in $Cl_{Ca}Cs$, despite otherwise large differences in channel properties. The hippocampal channel has a single-channel conductance of ~50 pS, and exhibits a nonlyotropic selectivity sequence ($NO_3 > I > Br > SCN > Cl > F$; Franciolini and Nonner, 1987), whereas $Cl_{Ca}Cs$ have a 25-fold smaller single-channel conductance (Takahashi et al., 1987; Hartzell, A., and A. Kuruma, unpublished observations) and very different relative selectivities. It is not immediately obvious how two pores large enough to accommodate complexes of large organic cations and anions can differ so dramatically in their throughput and selectivity. Clearly, electrostatic interactions between permeant anions and the pore walls must play a role because of the inability of cations to permeate in the absence of permeant anions. If anion permeation commonly occurs as cation–anion complexes, it will be necessary to rethink the mechanisms of anion permeation.

$Cl_{Ca}Cs$ Select between Anions Based only Partly on Hydration Energy

Many anion channels appear to select between anions based at least partly on their hydration energies (Franciolini and Petris, 1992; Smith et al., 1999; Dawson et al., 1999). Recently, Smith et al. (1999) have modeled the CFTR pore as a polarizable tunnel with a dielectric constant of ~20. Although this model provides valuable insights into the biophysical nature of the Cl channel pore in CFTR, we think that this model is inadequate in explaining the $Cl_{Ca}C$ channel permeation. One would expect that the barrier height would be linearly related to hydration energy if the pore were simply a polarizable tunnel. However, the barrier height appears to be exponentially related to the hydration energy (Fig. 6). Although anion channels, in general, are more permeant to anions with smaller hydration energies, the permeability sequences are different for different anion channels. Furthermore, the permeability sequences can be altered significantly by point mutations. For example, Fahlke et al. (1997c) showed that ClC-1 has a permeability sequence of $Cl > SCN > Br > NO_3 > I >$ methanesulfonate, and that this sequence can be altered to $SCN > NO_3 > I > Br > Cl >$ methanesulfonate by the G230E mutation. Other mutations in the highly conserved GKEGP sequence also have effects on anion permeation (Fahlke et al., 1997b). Smith et al. (1999) have proposed that CFTR may be a primitive type of anion channel with anion permeation being governed largely by partitioning of the anion into the hydrophilic environment of the pore, whereas other channels like ClC-1 may have other selectivity mechanisms superimposed that alter the selectivity sequence.

Channel Block and Anomalous Mole Fraction

Fig. 3 showed that anions with the highest and lowest permeabilities generally had the lowest conductances. This observation can be explained if one assumes that the ions with the lowest permeabilities do not easily enter the channel because of their large hydration energies, and that ions with the highest permeabilities enter the channel easily but bind to some site in the pore and, thus, do not easily permeate. The idea that there is a blocking site in the pore for permeant ions is supported by the observation that channel block by ions like $C(CN)_3$ are voltage-dependent (Figs. 7 and 8).

We propose that there are two binding sites for permeant anions in the pore for the following reasons. Woodhull analysis of the location of the binding site in the voltage field provides an estimate of 40% of the voltage field from the outside when $C(CN)_3$ is applied from the outside and 60% of the voltage field from the outside when $C(CN)_3$ is applied from the inside. It is possible that 40 and 60% are not different within the errors of our measurements, and that there is only one binding site approximately half-way across the voltage field. However, we favor the interpretation that there are actually two sites because analysis of the block of the current by high pH also predicts that there are two sites 40 and 60% across the voltage field. The fact that

we find that both $C(CN)_3$ and pH block of the channel yield the same conclusion strengthens this interpretation that there are two anion binding sites 40 and 60% across the voltage field.

If there are two anion binding sites in the pore, one would expect the channel to exhibit anomalous mole fraction behavior if the anions in these two sites interact. Evidence for anomalous mole fraction behavior of this channel, however, was ambiguous. With $C(CN)_3$ the conductance decreased monotonically with increasing $C(CN)_3$ concentration, but with SCN there was a minimum in the conductance at 25 mol% SCN. With $C(CN)_3$ the E_{rev}s and the relative permeabilities deviated somewhat from those predicted from the GHK equation. The minima and deviations from the GHK prediction are consistent with the suggestion that two ions may interact in the pore, but the deviations from predictions were not as prominent as has been described for other types of channels, such as voltage-gated Ca^{2+} channels (Almers and McCleskey, 1984; Hille, 1992). It may be that the anion binding sites in the pore are sufficiently far apart that interactions between anions are small.

We thank Nael McCarty, Shawn Zeltwanger, Zhiren Zhang, Dave Dawson, and Steve Smith for helpful discussion and comments, and Alyson Ellingson for technical assistance.

This study was supported by grants from the National Institutes of Health (GM-60448 and GM-55276).

Submitted: 30 May 2000
Revised: 18 September 2000
Accepted: 24 October 2000

REFERENCES

Almers, W., and E.W. McCleskey. 1984. Non-selective conductance in calcium channels of frog muscle: calcium selectivity in a single-file pore. *J. Physiol.* 353:585–608.

Amédéé, T., W.A. Large, and Q. Wang. 1990. Characteristics of chloride currents activated by noradrenaline in rabbit ear artery cells. *J. Physiol.* 428:501–516.

Begenisich, T., and J.E. Melvin. 1998. Regulation of chloride channels in secretory epithelia. *J. Membr. Biol.* 163:77–85.

Blatz, A.L., and K.L. Magleby. 1985. Single chloride-selective channels active at membrane resting potentials in culture rat skeletal muscle. *Biophys. J.* 47:119–123.

Bormann, J., O.P. Hamill, and B. Sakmann. 1987. Mechanism of anion permeation through channels gated by glycine and γ-aminobutyric acid in mouse cultured spinal neurones. *J. Physiol.* 385: 243–286.

Callamaras, N., and I. Parker. 2000. Ca^{2+}-dependent activation of Cl^- currents in *Xenopus* oocytes is modulated by voltage. *Am. J. Physiol.* 278:C667–C675.

Clapp, L.H., J.L. Turner, and R.Z. Kozlowski. 1996. Ca^{2+}-activated Cl^- currents in pulmonary arterial myocytes. *Am. J. Physiol.* 270: H1577–H1584.

Cliff, W.H., and R.A. Frizzell. 1990. Separate Cl^- conductances activated by cAMP and Ca^{2+} in Cl^- secreting epithelial cells. *Proc. Natl. Acad. Sci. USA.* 87:4956–4960.

Collier, M.L., P.C. Levesque, J.L. Kenyon, and J.R. Hume 1996. Unitary Cl^- channels activated by cytoplasmic Ca^{2+} in canine ventricular myocytes. *Circ. Res.* 78:936–944.

Cunningham, S.A., M.S. Awayda, J.K. Bubien, I.I. Ismailov, M.P. Arrate, B.K. Berdiev, D.J. Benos, and C.M. Fuller. 1995. Cloning of an epithelial chloride channel from bovine trachea. *J. Biol. Chem.* 270:31016–31026.

Dascal, N. 1987. The use of *Xenopus* oocytes for the study of ion channels. *CRC Crit. Rev. Biochem.* 22:317–387.

Dawson, D.C., S.S. Smith, and M.K. Mansoura. 1999. CFTR: mechanism of anion conduction. *Physiol. Rev.* 79(Suppl.):S47–S75.

Evans, M.G., and A. Marty. 1986. Calcium-activated chloride currents in isolated cells from rat lacrimal gland. *J. Physiol.* 378:437–460.

Fahlke, C., C. Dürr, and A.L. George Jr. 1997a. Mechanism of ion permeation in skeletal muscle chloride channels. *J. Gen. Physiol.* 110:551–564.

Fahlke, C., H.T. Yu, C.L. Beck, T.H. Rhodes, and A.L. George Jr. 1997b. Pore-forming segments in voltage-gated chloride channels. *Nature.* 390:529–532.

Fahlke, C., C.L. Beck, and A.L. George Jr. 1997c. A mutation in autosomal dominant myotonia congenita affects pore properties of the muscle chloride channel. *Proc. Nat. Acad. Sci. USA.* 94:2729–2734.

Franciolini, F., and W. Nonner. 1987. Anion and cation permeability of a chloride channel in rat hippocampal neurons. *J. Gen. Physiol.* 90:453–478.

Franciolini, F., and A. Petris. 1992. Transport mechanisms in chloride channels. *Biochim. Biophys. Acta.* 1113:1–11.

Franciolini, F., and W. Nonner. 1994a. Anion–cation interactions in the pore of neuronal background chloride channels. *J. Gen. Physiol.* 104:711–723.

Franciolini, F., and W. Nonner. 1994b. A multi-ion permeation mechanism in neuronal background chloride channels. *J. Gen. Physiol.* 104:725–746.

Frings, S., D. Reuter, and S.J. Kleene. 1999. Neuronal Ca^{2+}-activated Cl^- channels: homing in on an elusive channel species. *Progr. Neurobiol.* 60:247–289.

Galzi, J.L., A. Devillers-Thiery, N. Hussy, S. Bertrand, and J.P. Changeux. 1992. Mutations in the channel domain of a neuronal nicotinic receptor convert ion selectivity from cationic to anionic. *Nature.* 359:500–505.

Gandhi, R., R.C. Eble, A.D. Gruber, K.D. Schreur, H.-L. Ji, C.M. Fuller, and B.U. Pauli. 1998. Molecular and functional characterization of a calcium-sensitive chloride channel from mouse lung. *J. Biol. Chem.* 273:32096–32101.

Gomez-Hernandez, J.-M., W. Stühmer, and A.B. Parekh. 1997. Calcium dependence and distribution of calcium-activated chloride channels in *Xenopus* oocytes. *J. Physiol.* 502:569–574.

Gruber, A.D., R.C. Elble, H.-L. Ji, K.D. Schreur, C.M. Fuller, and B.U. Pauli. 1998. Genomic cloning, molecular characterization, and functional analysis of human CLCA1, the first human member of the family of Ca^{2+}-activated Cl channel proteins. *Genomics.* 54:200–214.

Gruber, A.D., K.D. Schreur, H.-L. Ji, C.M. Fuller, and B.U. Pauli. 1999. Molecular cloning and transmembrane structure of hCLCA2 from human lung, trachea, and mammary gland. *Am. J. Physiol.* 276:C1261–C1270.

Halm, D.R., and R.A. Frizzell. 1992. Anion permeation in an apical membrane chloride channel of a secretory epithelial cell. *J. Gen. Physiol.* 99:339–366.

Hartzell, H.C., K. Machaca, and Y. Hirayama. 1997. Effects of adenophostin-A and inositol-1,4,5-trisphosphate on Cl− currents in *Xenopus laevis* oocytes. *Mol. Pharmacol.* 51:683–692.

Hille, B. 1992. Ionic Channels of Excitable Membranes. 2nd ed. Sinauer Associates, Inc., Sunderland, MA. 607 pp.

Hirakawa, Y., M. Gericke, R.A. Cohen, and V.M. Bolotina. 1999. Ca^{2+}-dependent Cl^- channels in mouse and rabbit aortic smooth muscle cells: regulation by intracellular Ca^{2+} and NO. *Am. J. Phys-*

iol. 277:H1732–H1744.

Huang, S.J., W.O. Fu, Y.W. Chung, T.S. Zhou, and P.Y.D. Wong. 1993. Properties of cAMP-dependent and Ca^{2+}-dependent whole cell Cl^- conductances in rat epididymal cells. *Am. J. Physiol.* 264: C794–C802.

Hume, R.I., and S.A. Thomas. 1989. A calcium- and voltage-dependent chloride current in developing chick skeletal muscle. *J. Physiol.* 417:241–261.

Ishikawa, T., and D.I. Cook. 1993. A Ca^{2+}-activated Cl^- current in sheep parotid secretory cells. *J. Membr. Biol.* 135:261–271.

Jaffe, L.A., and N.L. Cross. 1986. Electrical regulation of sperm-egg fusion. *Annu. Rev. Physiol.* 48:191–200.

Ji, H.-L., M.D. DuVall, H.K. Patton, C.L. Satterfield, C.M. Fuller, and D.J. Benos. 1998. Functional expression of a truncated Ca^{2+}-activated Cl^- channel and activation by phorbol ester. *Am. J. Physiol.* 274:C455–C464.

Keramidis, A., A.J. Moorhouse, C.R. French, P.R. Schofield, and P.H. Barry. 2000. M2 pore mutations convert the glycine receptor channel from being anion to cation-selective. *Biophys. J.* 78:247–259.

Kozak, J.A., and D.E. Logothetis. 1997. A calcium-dependent chloride current in insulin-secreting βTC-3 cells. *Pflügers Arch.* 433: 679–690.

Kurahashi, T., and K.-W. Yau. 1994. Olfactory transduction: tale of an unusual chloride current. *Curr. Biol.* 4:231–237.

Kuruma, A., and H.C. Hartzell. 1999. Dynamics of calcium regulation of chloride currents in *Xenopus* oocytes. *Am. J. Physiol.* 276: C161–C175.

Kuruma, A., and H.C. Hartzell. 2000. Bimodal control of a Ca^{2+}-activated Cl^- channel by different Ca^{2+} signals. *J. Gen. Physiol.* 115:59–80.

Läuger, P. 1973. Ion transport through pores: a rate-theory analysis. *Biochim. Biophys. Acta.* 311:423–441.

Linsdell, P., and J.W. Hanrahan. 1998. Adenosine triphosphate dependent assymmetry of anion permeation in the cystic fibrosis transmembrane regulator chloride channel. *J. Gen. Physiol.* 111: 601–614.

Linsdell, P., J.A. Tabcharani, J.M. Rommens, Y.-X. Hou, X.-B. Chang, L.-C. Tsui, J.R. Riordan, and J.W. Hanrahan. 1997a. Permeability of wild-type and mutant cystic fibrosis transmembrane conductance regulator chloride channels to polyatomic anions. *J. Gen. Physiol.* 110:355–364.

Linsdell, P., J.A. Tabcharani, and J.W. Hanrahan. 1997b. Multi-ion mechanism for ion permeation and block in the cystic fibrosis transmembrane conductance regulator chloride channel. *J. Gen. Physiol.* 110:365–377.

Machaca, K., and H.C. Hartzell. 1998. Asymmetrical distribution of Ca-activated Cl channels in *Xenopus* oocytes. *Biophys. J.* 74:1286–1295.

Machaca, K., and H.C. Hartzell 1999a. Reversible Ca^{2+} gradients between the subplasmalemma and cytosol differentially activate two distinct Cl channel effectors. *J. Gen. Physiol.* 113:249–266.

Machaca, K., and H.C. Hartzell. 1999b. Adenophostin A and inositol 1,4,5-trisphosphate differentially activate Cl^- currents in *Xenopus* oocytes because of disparate Ca^{2+} release kinetics. *J. Biol. Chem.* 274:4824–4831.

Mansoura, M.K., S.S. Smith, A.D. Choi, N.W. Richards, T.V. Strong, M.L. Drumm, F.S. Collins, and D.C. Dawson. 1998. Cystic fibrosis transmembrane conductance regulator (CFTR) anion binding as a probe of the pore. *Biophys. J.* 74:1320–1332.

Marcus, Y. 1997. Ion Properties. Marcel Dekker, New York. 259 pp.

Morris, A.P. 1999. The regulation of epithelial cell cAMP- and calcium-dependent chloride channels. *Adv. Pharmacol.* 46:209–251.

Neher, E. 1992. Correction for liquid junction potentials in patch clamp experiments. *Methods Enzymol.* 207:123–131.

Nonner, W., D.P. Chen, and B. Eisenberg. 1998. Anomalous mole fraction effect, electrostatics, and binding in ionic channels. *Biophys. J.* 74:2327–2334.

Pusch, M., U. Ludewig, A. Rehfeldt, and T.J. Jentsch. 1995. Gating of the voltage-dependent chloride channel ClC-0 by the permeant anion. *Nature.* 373:527–531.

Rychkov, G.Y., M. Pusch, D.S. Astill, M.L. Roberts, T.J. Jentsch, and A.H. Bretag. 1996. Concentration and pH dependence of skeletal muscle chloride channel ClC-1. *J. Physiol.* 497.2:423–435.

Rychkov, G.Y., M. Pusch, M.L. Roberts, T.J. Jentsch, and A.H. Bretag. 1998. Permeation and Block of the skeletal muscle chloride channel ClC-1 by foreign anions. *J. Gen. Physiol.* 111:653–665.

Smith, S.S., E.D. Steinle, M.E. Meyerhoff, and D.C. Dawson. 1999. Cystic Fibrosis Transmembrane Conductance Regulator: physical Basis for Lyotropic Anion Selectivity Patterns. *J. Gen. Physiol.* 114: 799–817.

Tabcharani, J.A., P. Linsdell, and J.W. Hanrahan. 1997. Halide permeation in wild-type and mutant cystic fibrosis transmembrane conductance regulator chloride channels. *J. Gen. Physiol.* 110: 341–354.

Takahashi, T., E. Neher, and B. Sakmann. 1987. Rat brain serotonin receptors in *Xenopus* oocytes are coupled by intracellular calcium to endogenous channels. *Proc. Natl. Acad. Sci. USA.* 84:5063–5067.

Tsien, R.Y., and T. Pozzan. 1989. Measurements of cytosolic free Ca^{2+} with Quin-2. *Methods Enzymol.* 172:230–262.

Wang, C.-T., H.-G. Zhang, T.A. Rocheleau, R.H. ffrench-Constant, and M.B. Jackson. 1999. Cation permeability and cation-anion interactions in a mutant GABA-gated chloride channel from *Drosophila. Biophys. J.* 77:691–700.

Wang, Q., and W.A. Large. 1991. Noradrenaline-evoked cation conductance recorded with the nystatin whole-cell method in rabbit portal vein cells. *J. Physiol.* 435:21–39.

Woodhull, A.M. 1973. Ionic blockage of sodium channels in nerve. *J. Gen. Physiol.* 61:687–708.